Force-dependent ligand sensing enables αVβ3 integrin to differentiate between fibronectin and high-affinity ligands

Michael Bachmann[1,*], Markus Schäfer[1,2,*], Kai Weißenbruch[1], Vasyl V. Mykuliak[3], Lia Heiser[1], Clemens M. Franz[4], Vesa P. Hytönen[3], Bernhard Wehrle-Haller[5,6], Martin Bastmeyer[1,2,6]

Affiliations:
1: Zoological Institute, Cell- and Neurobiology, Karlsruhe Institute of Technology (KIT), Karlsruhe, Germany
2: Institute of Functional Interfaces (IFG), Karlsruhe Institute of Technology (KIT), Karlsruhe, Germany
3: Faculty of Medicine and Life Sciences and BioMediTech, University of Tampere, Finland and Fimlab Laboratories, Tampere, Finland
4: DFG–Center for Functional Nanostructures, Karlsruhe Institute of Technology (KIT), Karlsruhe, Germany
5: Department of Cell Physiology and Metabolism, University of Geneva, Geneva, Switzerland
6: Correspondence should be addressed to B. Wehrle-Haller (Bernhard.Wehrle-Haller@unige.ch) or M. Bastmeyer (martin.bastmeyer@kit.edu).
*: These authors contributed equally.

Abstract:
αVβ3 Integrin recognizes multiple extracellular matrix proteins, including vitronectin (Vn) and fibronectin (Fn). Binding of αVβ3 to these proteins causes different signaling events but it is unclear how this integrin selects for different ligands in a complex *in vivo* environment. Here, we employed binary-choice substrates of Fn and Vn to dissect αVβ3-mediated binding to both ligands on the subcellular scale. Super-resolution live-cell imaging revealed that αVβ3-mediated adhesions on binary Fn/Vn substrates exclusively initiate on Vn. Also, biochemical binding assays confirmed higher affinity of αVβ3 for Vn compared to Fn. During adhesion maturation, αVβ3-mediated contacts translocate to Fn depending on a force-mediated opening of the β3 headpiece. Thus, αVβ3 shows a force- and conformation-dependent ligand sensing enabling this integrin to differentiate between Fn and high-affinity ligands like Vn, osteopontin, and fibrinogen. This was also confirmed on soft substrates offering an explanation how αVβ3 selects between Fn and Vn in complex tissue environments.

Keywords:
Integrin, ECM, integrin affinity, outside-in signaling, mechanotransduction, mechanosensing, superresolution microscopy

List of abbreviations:
Fbg, fibrinogen; Fn, fibronectin; FnIII10, 10th domain of fibronectin; MEF, mouse embryonic fibroblast; MEF vcl -/-, mouse embryonic fibroblasts derived from vinculin knockout mice; MD, molecular dynamics; NMIIA, nonmuscle myosin IIA; Opn, osteopontin; Vn, vitronectin;

Introduction:
Integrins, an important class of cell-matrix adhesion receptors, consist of α- and β-subunits forming transmembrane heterodimers (Campbell and Humphries, 2011). While the extracellular part binds to proteins of the extracellular matrix (ECM), the intracellular part is connected to actin via multiple adapter and signaling proteins that make up the so-called adhesome (Hytönen and Wehrle-Haller, 2014, Zaidel-Bar et al., 2007a). Integrin activation on the functional level describes the capacity to bind ligands. On the structural level, activation is associated with conformational changes from a bent, to an extended-closed, and finally to an extended-open state (Campbell and Humphries, 2011, Zhu et al., 2008, Su et al., 2016). Concerning the β-integrin subunit, the extended-open conformation is reflected by the swing-out of the hybrid domain in respect to the βA domain (Zhu and Springer, 2013). Molecular dynamics (MD) simulations indicate that force supports this hybrid domain swing-out and thereby leads to full integrin activation (Zhu et al., 2008, Puklin-Faucher et al., 2006, Dong et al., 2017). These theoretical studies are supported by multiple examples where mechanical forces regulate integrin functions, structural elements of the adhesome, and thus integrin-mediated adhesions (Balaban et al., 2001, Stricker et al., 2011, Hytonen and Wehrle-Haller, 2016, Nordenfelt et al., 2016, Rahikainen et al., 2017, Kuo et al., 2011, Schiller et al., 2011).
The best-studied class of integrins is the group of RGD-binding integrins sharing the ability to interact with an exposed Arg-Gly-Asp peptide in their ligands (Hynes, 2002). Promiscuity between ligands and receptors is especially common for these RGD-integrins. For example, αVβ3 integrin is reported to have the ability to recognize at least 12 different ligands (Humphries et al., 2006). Initially described as

the vitronectin (Vn) receptor (Pytela et al., 1985), αVβ3 integrin is now widely accepted and analyzed in its function as a fibronectin (Fn) receptor (Roca-Cusachs et al., 2009, Schiller et al., 2013, Cao et al., 2017, Danen et al., 2002, Balcioglu et al., 2015). The importance of Fn binding by αVβ3 integrin is supported by developmental defects in knockout mice (Yang et al., 1999) and by cancer-associated fibroblasts that need αVβ3 integrin for migration and rearrangement of Fn (Attieh et al., 2017, Erdogan et al., 2017). In contrast, αVβ3 integrin binding to Vn mediates pro-angiogenic effects (Li et al., 2014) and cross-activates the VEGF receptor (Soldi et al., 1999, West et al., 2012). Thus, it appears that αVβ3 integrin mediates different activities dependent on the ligand. However, a mechanistic understanding how αVβ3 integrin selects from different available ligands when exposed to a more complex ECM remains ambiguous.
We have recently developed a method to produce microstructured, differential Fn/Vn substrates that enable us to analyze the influence of Fn and Vn coated surfaces on a subcellular scale (Pinon et al., 2014, Rahikainen et al., 2017). Here, we combine this method with super-resolution microscopy and super-resolution live cell imaging and reveal a force dependent ligand sensing that permits αVβ3 integrin to discriminate between Fn and Vn. Furthermore, we show that this sensing occurs over a physiological range of tissue stiffness. And finally, we reveal that Vn, together with osteopontin (Opn) and fibrinogen (Fbg), belongs to a class of high-affinity ligands for αVβ3 integrin contrasting with the low-affinity ligand Fn.

Results:

Vitronectin is the preferred ligand for αVβ3 integrin
To study how the simultaneous presentation of two ECM ligands influences binding of αVβ3 integrin, we produced binary Fn/Vn substrates with subcellular structural resolution (Pinon et al., 2014). 2x2 µm squares of Fn separated by 1 µm gaps were stamped onto a coverslip and the remaining surface was covered with Vn leading to a geometrical coverage of about equal contribution (Pinon et al., 2014). The quality of substrates was analyzed by fluorescence and atomic force microscopy (Fig. 1a, b). To reveal integrin specific ECM ligand binding, β3-wt integrin GFP was transfected into NIH 3T3 cells expressing low levels of endogenous β3 integrins, and cultured on the patterned surfaces for 2 hrs (Pinon et al., 2014). Subsequent fixation and immunostaining for paxillin allowed detecting all integrin-mediated cell-matrix adhesions. Imaging with super-resolution structured illumination microscopy (SR-SIM) revealed extended overlap of αVβ3 integrin and anti-paxillin staining (Fig. 1c). However, some paxillin-clusters on Fn were free of αVβ3 integrin, indicating recruitment to endogenous Fn-bound α5β1 integrin (Supplementary Fig. 1b, g). Therefore, these substrates enabled us to analyze the influence of Fn and Vn on αVβ3 integrin adhesion formation at a micrometer scale within single cells. Surprisingly, we found a clear preference of αVβ3 integrin-positive adhesions for Vn with 83.5 % colocalization (Fig. 1d). This preference for Vn was independent of the size of the αVβ3 integrin-mediated adhesion (Fig. 1e), the presence of α5β1 integrin (Supplementary Fig. 1a, f), or the stamping procedure (Supplementary Fig. 1d, j). The preference was also confirmed on homogenous substrates, where the degree of αVβ3-integrin recruitment into adhesions was increased on Vn compared to Fn (Supplementary Fig. 2). To study the dynamics of αVβ3 integrin-mediated adhesion formation, we applied SR-SIM live cell imaging. During spreading, cells initiated numerous nascent adhesions (Fig. 1g and Supplementary Video 1 and 2). These adhesions almost exclusively appeared on Vn (Fig. 1f) while some of them were later translocated towards Fn in a centripetal direction towards the cell center (Fig. 1g and Supplementary Video 2). In control experiments where Fn was replaced by albumin, αVβ3 integrin-mediated adhesions were constrained to Vn (Supplementary Fig. 1c), indicating that ligand binding was necessary for localization and stabilization of αVβ3 integrins on Fn-coated squares. Next, we asked whether the preference for Vn could be explained by different affinities of αVβ3 integrin for these two ligands. Using biolayer interferometry, we analyzed the dissociation constant of purified αVβ3 integrins for Fn and Vn (Fig. 1h, i). Remarkably, Vn showed dissociation from αVβ3 integrins only in the presence of the αVβ3 integrin inhibitor cilengitide (w/o cilengitide: K_d < 1 pM; + 20 µM cilengitide: K_d = 302.6 nM; Supplementary Fig. 3b), which was similar to previous reports showing non-dissociable binding to Vn (Orlando and Cheresh, 1991). Fn, in contrast, dissociated rapidly (K_d = 53.98 nM), proposing that the higher affinity of the extracellular domain of αVβ3 integrin for Vn explains the observed Vn-preference. Accordingly, a chimeric integrin with extracellular β3 and intracellular β1 domains (β3/β1 chimera) showed the same preference for Vn as β3-wt integrin on the micropatterned Fn/Vn surfaces (Supplementary Fig. 1e, h), emphasizing the importance of outside-in signaling in the process of differential ligand recognition. In addition, we performed atomic force microscopy (AFM)-based single-cell force spectroscopy (Langhe et al., 2016, Dao et al., 2012) on substrates with adjacent Fn and Vn areas. A living cell attached to the AFM cantilever was alternatingly brought in contact with and retracted from two homogenously coated but adjacent Fn and Vn areas. In respect to different contact times (typically ten force cycles per cell and contact time), the

detachment force was determined from force-distance curves collected during cell retraction. Starting after 30 s of adhesion time, a significantly higher force was needed to detach cells from Vn compared to Fn substrates (Fig. 1j).
Together, our experiments revealed that initial αVβ3 integrin-mediated adhesions formed exclusively on Vn, potentially explained by the higher binding affinity of αVβ3 integrin to Vn. However, the question remained why a portion of αVβ3 integrin-mediated adhesions still localized on Fn and how they were stabilized.

Actomyosin contractility regulates the ligand preference of αVβ3 integrin
To test whether mechanical forces are involved in the substrate selection process, we reduced actomyosin contractility with blebbistatin or Y27632. As previously shown (Choi et al., 2008), both inhibitors increased the number of small, round nascent adhesions in the cell periphery (Fig. 2a, b). In addition, treatment with both inhibitors led to a drastic decrease in colocalization of β3-wt GFP integrin with Fn (Fig. 2g and Supplementary Fig. 1k). Vinculin is well established as an important part of the molecular clutch to transmit forces from actin to the integrin-ECM bond (Thievessen et al., 2013, Humphries et al., 2007, Rahikainen et al., 2017). Therefore, we analyzed the localization of β3-wt GFP integrin on Fn/Vn substrates for mouse embryonic fibroblasts derived from vinculin knockout mice (MEF Vcl -/-). Indeed, the absence of vinculin led to a decrease in Fn binding of αVβ3 GFP integrin (Fig. 2e, h) that was comparable to the results obtained with the contractility inhibitors (Fig. 2g). Control experiments using wt MEFs (Fig. 2d) and Vcl -/- MEFs re-expressing vinculin mCherry (Fig. 2f) demonstrated that the localization of αVβ3 GFP integrin on Fn can be rescued by vinculin expression (Fig. 2h). To increase intracellular forces, we overexpressed nonmuscle myosin IIA mApple (NMIIA) in NIH3T3 cells (Fig. 2c). Indeed, adding additional NMIIA caused a significant increase of αVβ3 GFP integrin localization on Fn (Fig. 2g). Taken together, these findings indicate that αVβ3 integrin initially binds to Vn and that the subsequent binding of some of these integrins onto Fn requires intracellular forces and vinculin.

Hybrid-domain swing-out is important for fibronectin binding by αVβ3 integrin
Next, we asked why mechanical force stabilizes αVβ3 integrin-mediated adhesions on Fn, while initial αVβ3 integrin adhesions do not form on Fn when exposed to Fn/Vn substrates. It has been shown, that mechanical load enhances integrin activation by influencing the allosteric integrin regulation that leads to the complete hybrid domain swing-out in the headpiece of the β integrin subunit (Zhu et al., 2008, Ciobanasu et al., 2014, Humphries et al., 2007). Therefore, we determined the influence of the allosteric regulation of αVβ3 integrins on their ligand preference by using chemical activation (Fig. 3a) or established integrin mutations (Fig. 3b-d): (i) Mn^{2+} treatment shifts the integrin equilibrium to the extended-closed conformation (Li et al., 2017, Eng et al., 2011), (ii) the β3-VE mutant increases the affinity for talin 20-fold leading to increased integrin activation (Pinon et al., 2014), (iii) β3-D723A interrupts the inhibitory salt-bridge at the cytoplasmic side of the membrane between the αV- and β3-subunits (Saltel et al., 2009), and (iv) β3-N305T leads to a constitutive hybrid domain swing-out and slower integrin dynamics (Luo et al., 2003, Cluzel et al., 2005). On binary choice substrates, only β3-N305T expressing cells showed a significant increase of colocalization between αVβ3 GFP integrins and Fn (Fig. 3e), while Mn^{2+} treatment and the intracellular activating mutations (β3-VE and β3-D723A) caused no significant difference. However, and despite the enhanced localization on Fn surfaces, β3-N305T still localized preferentially on Vn (72.2% colocalization with Vn compared to 83.5% for β3-wt). Next, we tested whether the conformational changes caused by the β3-N305T mutation are accompanied by the ability to initiate adhesions on Fn by using live cell SR-SIM (Fig. 3f and Supplementary Video 3, 4) and compared this to the β3-VE mutation (Supplementary Video 5, 6). In both cases, spreading cells initiated most αVβ3 integrin-mediated adhesions on Vn. In contrast, only cells expressing β3-N305T were able to form also numerous adhesions on Fn (Fig. 3g). Interestingly, combining β3-wt + Mn^{2+} or the mutations β3-VE and β3-D723A with a blebbistatin treatment led to reduced localization of these integrins on Fn similar to β3-wt + blebbistatin (Supplementary Fig. 1l; unfortunately, β3-N305T could not be combined with blebbistatin treatment). Thus, allosteric activation to the extended closed conformation can not compensate for a loss in contractility concerning the choice of the extracellular ligand binding. When combined, the experiments above emphasize the crucial role of a force-mediated hybrid domain swing-out in the binding of αVβ3 integrin to Fn.
Concerning integrins under low force, we made a peculiar observation for all activating mutations and the Mn^{2+} treatment. In the cell center, we observed numerous small adhesions that localize almost exclusively on Vn (Fig. 3 a-d, Supplementary Fig. 4d). These αVβ3 integrin-mediated adhesions recruit talin but not paxillin, vinculin, or actin stress fibers indicating that they are not mechanically coupled and thus are under low intracellular force (Supplementary Fig. 4 a-c). Similar integrin clusters have been reported before to appear within minutes after Mn^{2+} addition (Cluzel et al., 2005, Saltel et

al., 2009). The exclusive localization of these low-force αVβ3 integrins on Vn complements our experiments using contractility inhibitors and vinculin -/- cells (Fig. 2g, h).
Combined, these experiments highlight the necessity of the extended-open conformation of αVβ3 integrin in Fn-binding on Fn/Vn substrates. In contrast, conditions that favor the extended-closed conformation do not lead to increased localization of αVβ3 integrin on Fn.

Molecular dynamics (MD) simulation confirm conformation-dependent Fn binding
Based on the correlation of extended-open conformation of αVβ3 integrin and Fn binding, we set out to understand this correlation on a structural, single protein level. Therefore, we employed molecular dynamics (MD) simulations. We investigated the binding of the RGD-containing 10th domain of Fn (FnIII10) to extended conformations of αVβ3 integrin exhibiting either the open or closed headpiece. The open headpiece is characterized by hybrid domain swing-out, inward movement of the N-terminal α1-helix, bearing MIDAS and ADMIDAS motifs, and by a piston-like motion of β6-α7 loop and α7-helix (Arnaout et al., 2007). For the MD simulation, a crystal structure of FnIII10-bound to the extended-closed conformation of αVβ3 integrin (PDB: 4MMX) was used as an initial model for FnIII10 binding to αVβ3 integrin. The structure of the extended-open form was prepared by superimposition of βA and hybrid domains from the crystal structure of open αIIbβ3 integrin. After initial short simulations, in order to select replicas based on FnIII10-orientation and interaction energy between the RGD-sequence of FnIII10 and αVβ3 integrin, we proceeded for 100 ns simulations. These MD simulations showed that the orientation of FnIII10 binding to the extended-closed conformation was different to the extended-open conformation (Fig. 4a). Several results support the necessity of an open αVβ3-headpiece for efficient Fn binding:

(i) An overlay of both integrin conformations with 9th and 10th domain of Fn showed that sterical clashes of full-length Fn and the αVβ3 integrin headpiece are likely for the extended-closed but not for the extended-open conformation (Supplementary Fig. 5a, b).
(ii) The α1-helix in FnIII10-bound αVβ3 integrin showed high flexibility in the extended-closed conformation compared to the open headpiece (Supplementary Fig. 5c). The higher flexibility was accompanied by a bent, broken α1-helix on the conformational level (Fig. 4a, b). Unbending of the α1-helix (Fig. 4b) is a common feature of headpiece opening in the integrin headpiece (Zhang et al., 2013). Differences in flexibility are less pronounced for unliganded αVβ3 integrin (Supplementary Fig. 5e).
(iii) Flexibility in the integrin in extended-closed conformation was mirrored in the RGD-peptide as shown by less stable interaction energy between FnIII10 and αVβ3 integrin (Fig. 4c), and by higher flexibility (Fig. 4d).
(iv) ADMIDAS interaction with the β6-α7 loop is an established indicator for the extended-closed conformation (Zhu and Springer, 2013). Indeed, our analysis of interactions between ADMIDAS and the β6-α7 loop showed that the loop interacted with the ADMIDAS metal ion preferentially in the extended-closed conformation of αVβ3 integrin (Supplementary Fig. 5d). This difference was specific for Fn-bound αVβ3 integrin (Supplementary Fig. 5f). Accordingly, decrease of ADMIDAS - β6-α7 loop interaction requires Fn-binding to the extended-open conformation.

Thus, these results suggest that FnIII10 - αVβ3 integrin binding is less stable in the extended-closed conformation, and becomes more stable once the integrin is in the extended-open form upon hybrid domain swing-out. This complements our experimental results on the correlation of extended-open conformation and Fn binding as shown by the β3-N305T mutation (Fig. 3e, g).

Mechanotransduction is influenced by the integrin/ligand combination
The acting forces on integrins are the combination of intracellular actomyosin contractility and the stiffness-dependent elastic responses of the extracellular matrix. When cells are plated onto substrates with different stiffness, an induction of cell spreading has only been observed on substrates with a Young's modulus E > 3-5 kPa (Yeung et al., 2005, Elosegui-Artola et al., 2016). However, a recent report showed that the activating mutation β3-VE led to cell spreading even on soft (E = 1.5 kPa) substrates (Pinon et al., 2014), implying that integrin activation determines mechanotransduction. These studies have been performed with cells expressing αVβ3 and α5β1 integrins cultured on Fn. We asked whether force-dependent Fn-binding of αVβ3 integrin may be a critical switch that allows αVβ3-dependent spreading on Fn surfaces only on stiffer substrates. Such an effect would be masked in cells expressing α5β1 integrins. Therefore, we employed β1 integrin-deficient GD25 cells and cultured them on elastic substrates with homogeneous Fn coating and compared them to Vn-coated substrates. Cell area and length of paxillin-positive adhesions in cells on both ligands correlated with the stiffness of the elastic gels (Fig. 5 a-f). A quantitative analysis revealed a sigmoidal switch for adhesion length and cell area on substrates with E = 5 kPa irrespective of the ligand (Fig. 5g and Supplementary Fig. 6b), suggesting that mechanosensing is regulated independent of integrin ligands. Another explanation could be that preference of αVβ3 integrins for Vn is only valid on glass

substrates. Therefore, we combined binary choice substrates with elastic gels (Supplementary Fig. 6a). For cells on soft gels (E ≤ 6.7 kPa), we could not reliably analyze the localization of adhesions on Fn/Vn substrates. However, this was possible on gels with intermediate stiffness, where αVβ3 integrin-mediated adhesions showed the same behavior as on glass (Fig. 5h, i). Paxillin, recruited by αVβ3 integrin in GD25 cells, colocalized with Fn to 15.5 % (E = 33 kPa), or 14.3 % (E = 219 kPa), respectively, confirming that αVβ3 integrin prefers Vn over a wide stiffness range.

Ligands of αVβ3 integrin belong to two different affinity regimes
Finally, we asked whether our findings for the interaction of αVβ3 integrin with Fn and Vn are also valid for other ligand combinations. We performed additional affinity measurements of αVβ3 integrin and its ligand fibrinogen (Fbg) revealing low dissociation and high ligand affinity (K_d = 8.15 ± 4.82 nM; Supplementary Fig. 4a, c) similar to the measurement for Vn (Fig. 1g, h). In addition, we produced binary choice substrates (Fig. 6c) to challenge αVβ3 integrin with Fn and Fbg (Fig. 6a) or with Fn and osteopontin (Opn; Fig. 6b). Interestingly, αVβ3 integrin colocalized with Fbg (Fig. 6d) or Opn (Fig. 6e) to the same amount as with Vn on Fn/Vn substrates (colocalization to Fn: 16.5% on Fn/Vn, 20.2% on Fn/Fbg, 18.3% on Fn/Opn). Next, we tested binary choice substrates composed of Vn/Fbg (Fig. 6f, j) or Vn/Opn (Fig. 6g, j) and analyzed αVβ3 integrin localization (Fig. 6h, i). On these substrates, αVβ3 integrin was unable to differentiate between both ligands (colocalization to Vn: 45.9% on Vn/Fbg, 50.4% on Vn/Opn). Thus, Vn, Opn, and Fbg may present a class of high-affinity ligands for αVβ3 integrin compared to the low-affinity ligand Fn.

Discussion

Here, we have analyzed the interaction of αVβ3 integrin with several established ligands. We showed that αVβ3 integrin clearly prefers binding to Vn, Fbg, and Opn in biochemical assays as well as in cell culture studies. Most surprising was the inability of αVβ3 integrin to initiate adhesions on Fn in the context of Fn/Vn substrates. Combined with the force-dependent localization of αVβ3 integrin from Vn to Fn, we introduce a hypothesis of force-dependent ligand binding that is supported by several experiments.

The vitronectin receptor
Our findings shed light on the decade old controversy of the binding specificity of αVβ3 integrin towards Vn, and Fn. When αVβ3 integrin was identified, it was coined “the vitronectin receptor” based on its ability to bind to Vn and, equally important, its inability to bind to Fn (Pytela et al., 1985). However, later it was shown that αVβ3 integrin also binds to Fn substrates when tested in a cellular context (Wennerberg et al., 1996). The data presented here explain these contradicting observations. Indeed, αVβ3 integrin binding under low forces is “the vitronectin receptor” (Fig. 7b) as Pytela and colleagues stated (Pytela et al., 1985). However, pulling on this integrin increases the ability to bind to Fn (Fig. 7c), thereby explaining the abundant examples of αVβ3 integrin acting as an Fn-receptor in cells and *in vivo*. This differential ligand sensing we presented here allows a re-interpretation of several important studies about αVβ3 and α5β1 integrin on Fn substrates. One well-established difference between these integrins is their subcellular localization in cells cultured on Fn (Zamir et al., 2000). αVβ3 integrin is enriched in peripheral focal adhesions compared to central fibrillar adhesions where α5β1 integrin dominates. Our data offers a surprisingly simple solution that is only based on the force levels in a cell. Fibrillar adhesions are described as low-contractile compared to focal adhesions (Zaidel-Bar et al., 2007b). This favors αVβ3 integrin only in focal adhesions with forces that are necessary for efficient Fn binding. In contrast, α5β1 integrin binds to its ligand Fn even in low-force fibrillar adhesions. More recently, it was stated that αVβ3 integrin is more force-sensitive (Schiller et al., 2013, Roca-Cusachs et al., 2009) and that single αVβ3 integrins are immobilized to a higher degree than α5β1 integrins (Rossier et al., 2012). Both reports fit to our data since reducing contractility affected αVβ3 integrin binding on its low-affinity ligand Fn more, than it might affect α5β1 integrin. On the other hand, single αVβ3 integrins that are bound to Fn are in a maximally-activated state explaining their spatial immobilization. Thus, the statements in these studies about αVβ3 integrin still hold true. But combined with our data, it becomes apparent that dynamics and regulation of αVβ3 integrin are highly ligand-dependent and that integrins should be analyzed with respect to their ligand.

Force-regulated conformation
Our experiments revealed a differential binding of αVβ3 integrin to Fn and Vn dependent on cellular forces pulling on αVβ3 integrin. On a structural level, our MD simulations of αVβ3 integrin emphasized that the extended-open conformation with hybrid domain swing-out was necessary for efficient Fn binding to αVβ3 integrin. Accordingly, cell experiments with ensembles of αVβ3 integrins only showed

increased localization on Fn in the context of the β3-N305T integrin causing extended-open conformation. It is obvious to speculate that Vn, in contrast to Fn, can already bind to the extended-closed conformation of αVβ3 integrin, which then progresses to the extended open conformation, similar to observations with αIIbβ3 integrin (Eng et al., 2011). Due to the lack of structural data on Vn, it was not possible to run MD simulations for αVβ3 integrin and Vn. But several indications support binding of Vn to the extended-closed conformation of αVβ3 integrin. First, this scenario would require a very flexible ligand, or ligand sequence exposed in a peptide. This would allow easier access to the RGD-binding site in the extended-closed, or even bent, conformation of αVβ3 integrin. Indeed, many high-affinity ligands for αVβ3 integrin exhibit their RGD-peptide in an extended-loop or non-structured context. In contrast, Fn exhibits its RGD-peptide in a short loop. Thus, steric constraints during ligand binding to αVβ3 integrin are more likely the case for the short RGD loop in Fn. Second, Mn^{2+} treatment activates integrins by shifting the equilibrium to the extended-closed but not to the extended-open conformation (Eng et al., 2011). On a cellular level, we showed that Mn^{2+} treatment leads to clustered, ligand-bound αVβ3 integrin clusters that exclusively localize on Vn whereas Fn binding was not increased by Mn^{2+}. Additionally, interfering with talin-integrin binding (D723A- and VE-mutation) leads to analogous effects. And third, several MD simulations predicted that pulling on the β-subunit of an integrin favors the extended-open conformation (Zhu et al., 2008, Puklin-Faucher et al., 2006, Dong et al., 2017). Accordingly, our data showed that increasing myosin IIA levels also increased Fn binding of αVβ3 integrin, whereas Vn binding was unaffected by decreased contractility.
In total, concerning the interaction of αVβ3 with Fn, we present here a correlation of force and integrin activation that was predicted by MD simulations for different integrins (Zhu et al., 2008, Puklin-Faucher et al., 2006, Dong et al., 2017) and that was experimentally supported for αLβ2 integrin (Nordenfelt et al., 2016). More importantly, concerning Fn and Vn, we showed that the force-regulated conformation of αVβ3 integrin allows a differential ligand sensing. This adds a completely new facet to the force-conformation relationship in integrins.

Inside-out mechanosensing

Inside-out signaling in mechanotransduction is well documented especially via the paxillin-FAK signaling axis (Shikata et al., 2005, Plotnikov et al., 2012). Indeed, Pinon and colleagues (Pinon et al., 2014) have shown that paxillin recruitment by an integrin-talin-interface is necessary for spreading on soft substrates. However, the importance of ligand-dependent outside-in signaling let us expect that mechanotransduction via αVβ3 integrin differs for Fn compared to Vn. Surprisingly, based on focal adhesion length and cell area, we observed a mechanoswitch unaffected by the ligand and comparable to earlier reports using cells expressing different integrins (Elosegui-Artola et al., 2016, Yeung et al., 2005). Thus, concerning mechanotransduction, inside-out signaling dominates over outside-in signaling via integrin ligands. In contrast, the preference of αVβ3 integrin for Vn over a large range of ECM stiffness (Fig. 5i) indicates that outside-in signaling determines ligand recognition. The dominance of cellular parameters and inside-out signaling for the 5 kPa mechanoswitch is also confirmed by theoretical considerations about mechanosensing by cells (Schwarz, 2017).
Therefore, αVβ3 integrin contributes to mechanosensing irrespective of the ligand but robustly binds to Vn irrespective of the stiffness. Accordingly, *in vivo,* αVβ3 integrin will switch from Fn to Vn binding (or to Opn or to Fbg) whenever a high-affinity ligand becomes available.

The vitronectin receptor *in vivo*

What are the consequences of our findings for αVβ3 integrin *in vivo*? Vn and Fn are found circulating in the blood stream at similar concentrations (200-300 µg/ml; Izumi et al., 1989, Pankov and Yamada, 2002) whereas healthy tissue contains Fn but not Vn. Accordingly, αVβ3 integrin in fibroblasts in connective tissue will bind to Fn and contribute to cell adhesion. However, a wound will bring Vn into the connective tissue leading to a shift of αVβ3 integrin from Fn to Vn. This will concentrate Vn in the wound where it orchestrates blood clotting and fibrinolysis together with PAI-1 (Preissner and Reuning, 2011). On the other side, endothelial cells in sprouting vessels, in contrast to mature vessels, express αVβ3 integrin. Vn together with VEGF has pro-angiogenic effects (Li et al., 2014) that might be explained by cross-activation between the VEGF receptor 2 and αVβ3 integrin (Soldi et al., 1999, West et al., 2012). Our data now imply that αVβ3 integrin specifically recruits Vn from the blood, largely ignoring Fn that is present at similar concentrations. In this setting, force-dependent ligand sensing potentially facilitates selective binding to Vn since soluble, unattached Fn might not exert sufficient forces to cause the extended-open conformation of αVβ3 integrin. Beside pro-angiogenic effects, selective Vn binding by endothelial cells might also serve as an additional protection from thrombus formation. Vn, in contrast to Fn, is a matricellular protein unable to build a ECM meshwork and accordingly a thrombus.

Based on our data, Vn, Opn, and Fbg emerge as preferred ligands for αVβ3 integrin in contrast to Fn. At the same time, only αV/α5 integrin double knockout mice mimick the developmental defects of Fn knockout mice. This illustrates the physiological importance of Fn binding by αVβ3 integrin (Yang et al., 1999). Binding high-affinity ligands compared to Fn also causes different cellular outcomes. Vn binding by αVβ3 integrin, as mentioned in the examples above, regulates blood clotting, fibrinolysis, and angiogenesis. In contrast, in cancer-associated fibroblasts, αVβ3 integrin is reported to assemble and rearrange Fn (Attieh et al., 2017) and to increase migration speed on Fn (Erdogan et al., 2017). Thus, in the latter case, αVβ3 integrin mediates cell adhesion and migration while Vn as ligand leads to non-classical integrin functions in wound healing or angiogenesis. Accordingly, the combination of integrins with a specific ligand emerges as an additional regulatory layer in integrin signaling. This increases the possibilities of integrin-mediated outside-in signaling and might be especially true for the promiscuous αVβ3 integrin. Accordingly, we assume that analyzing ligand-dependent influences on integrin signaling offers a new avenue for a better understanding of integrins in *in vivo* settings characterized by a complex ECM composition.

Acknowledgements:

This work was supported by the German Research Foundation (Karlsruhe School of Optics and Photonics (KSOP) to M. Bachmann) and by the Baden-Württemberg Stiftung (State Scholarship to M. Schäfer). We thank Academy of Finland for financial support (grant no. 290506 to V. Hytönen) and acknowledge CSC – IT center for science for computational resources and EDUFI (former CIMO) for postdoctoral fellowship for V. Mykuliak. Swiss National Science Foundation supported the work of B. Wehrle-Haller (31003A_166384). The authors declare no competing financial interests.

Author contributions:

M. Bachmann, B. Wehrle-Haller, and M. Bastmeyer conceived the study. M. Bachmann, M. Schäfer, V. Hytönen, B. Wehrle-Haller, and M. Bastmeyer designed the experiments, M. Bachmann, M. Schäfer, K. Weißenbruch, V. Mykuliak, L. Heiser, and C. M. Franz performed and analyzed the experiments. M. Bachmann, M. Schäfer, B. Wehrle-Haller, and M. Bastmeyer wrote the paper. All authors discussed the results and implications and commented on the manuscript.

Figures:

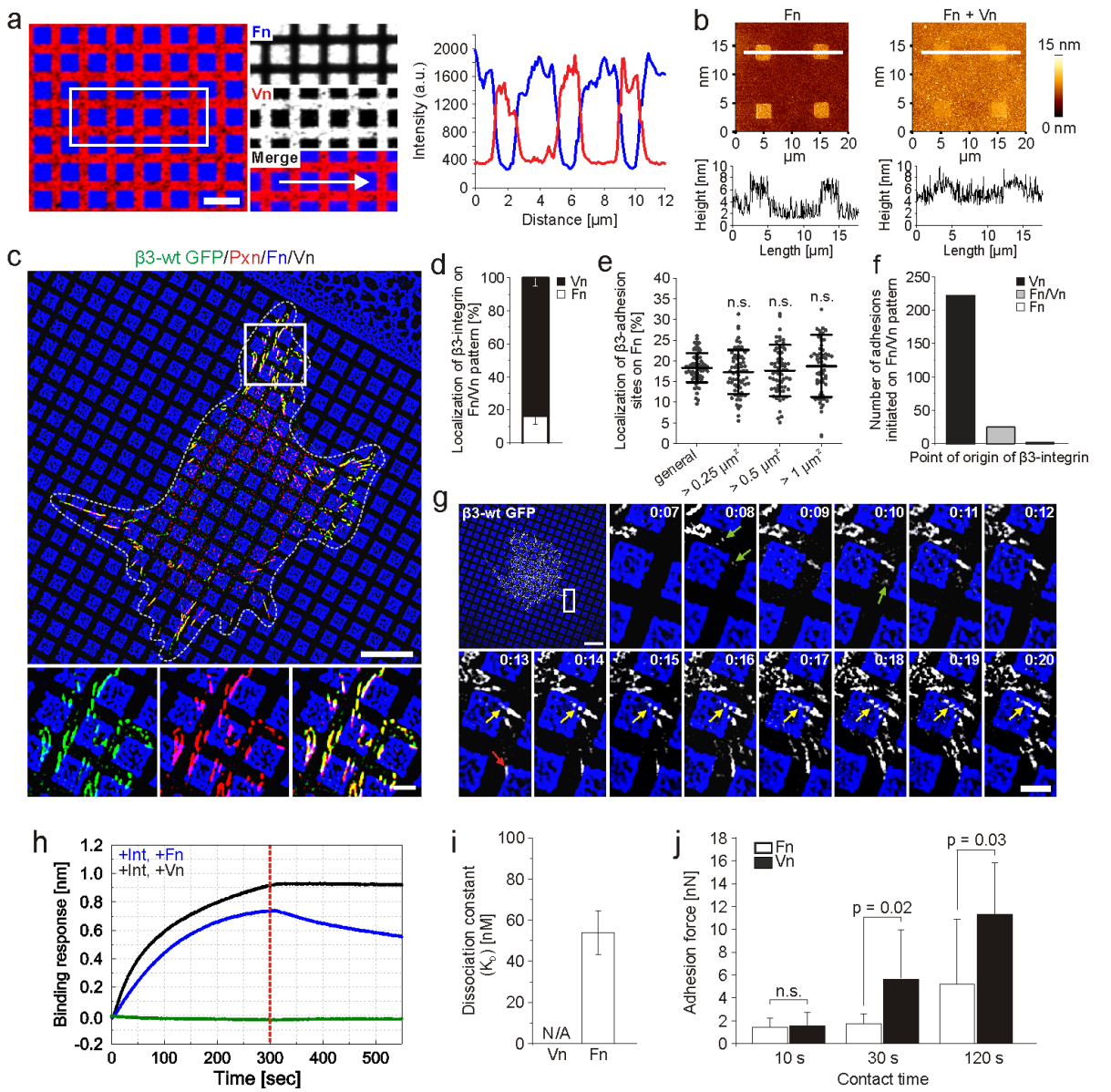

Figure 1: αVβ3 integrin favors binding to vitronectin (Vn) compared to fibronectin (Fn). (**a**) Microcontact printing of 2x2 µm squares of Alexa Fluor 647 labeled Fn (blue) onto glass cover slips and backfilling the pattern with Alexa Fluor 568 labeled Vn (red) leads to differential Fn/Vn patterns as shown by the fluorescence intensity profile along the arrow. Geometrical coverage varies dependent on the pattern quality: 44-49% Fn, 56-51% Vn. (**b**) Height profiles of Fn patterns (left) and Fn/Vn patterns (right) measured with atomic force microscopy (AFM) in contact mode. Profiles along the white lines indicate a monolayer of Fn and a uniform topography of the binary choice substrates. (**c**) Super-resolution structured illumination microscopy (SR-SIM) image of a NIH 3T3 cell transfected with β3-wt GFP integrin (green), cultured on a Fn/Vn pattern (Fn in blue), and immunostained for paxillin (red). The cell contour is outlined with a dashed white line. (**d**) Quantification of colocalization of β3-wt GFP integrin with Fn or Vn for fixed cells (n = 66; N = 4). (**e**) Quantification of colocalization of β3-wt GFP integrin with Fn for all adhesions ("general") or only for those longer than the indicated threshold (re-analysis of the data from **d**). (**f**) Total number of αVβ3-mediated adhesions that initiated on Vn, Fn, or at the Fn/Vn-interface for cells imaged with live cell SR-SIM. Quantification is based on 246 initiated adhesions from six cells out of three independent experiments. (**g**) NIH 3T3 cell transfected with β3-wt GFP integrin (white) seeded on Fn/Vn patterns (Fn in blue) was monitored with live cell SR-SIM (also see Supplementary Video 1). Magnifications show initiation and maturation of αVβ3-mediated adhesions (time is given in h:min). Green arrows point to newly established adhesions. Yellow arrows follow adhesions that initiated on Vn while they translocate to Fn. The red arrow at 13 min indicates an

adhesion that appeared at the Fn/Vn-interface. (**h**) Representative curves for Fn and Vn association (0 sec to 300 sec) and dissociation (300 sec to 550 sec) to αVβ3 integrin measured with biolayer interferometry. (**i**) K_d values for the interaction of purified αVβ3 integrin to Vn or Fn measured with biolayer interferometry (values calculated from n = 9 measurements in N = 3 independent experiments). (**j**) Single-cell force spectroscopy of GD25 cells (expressing αVβ3, but no β1 integrin). Detachment forces on Fn and Vn measured after the indicated contact time points. Typically 10 force measurement repetitions were performed for each cell and time point, and a total of 8 cells were tested. (**a, c, d**) Scale bars: 10 µm in overviews, 2 µm in zoom-ins.

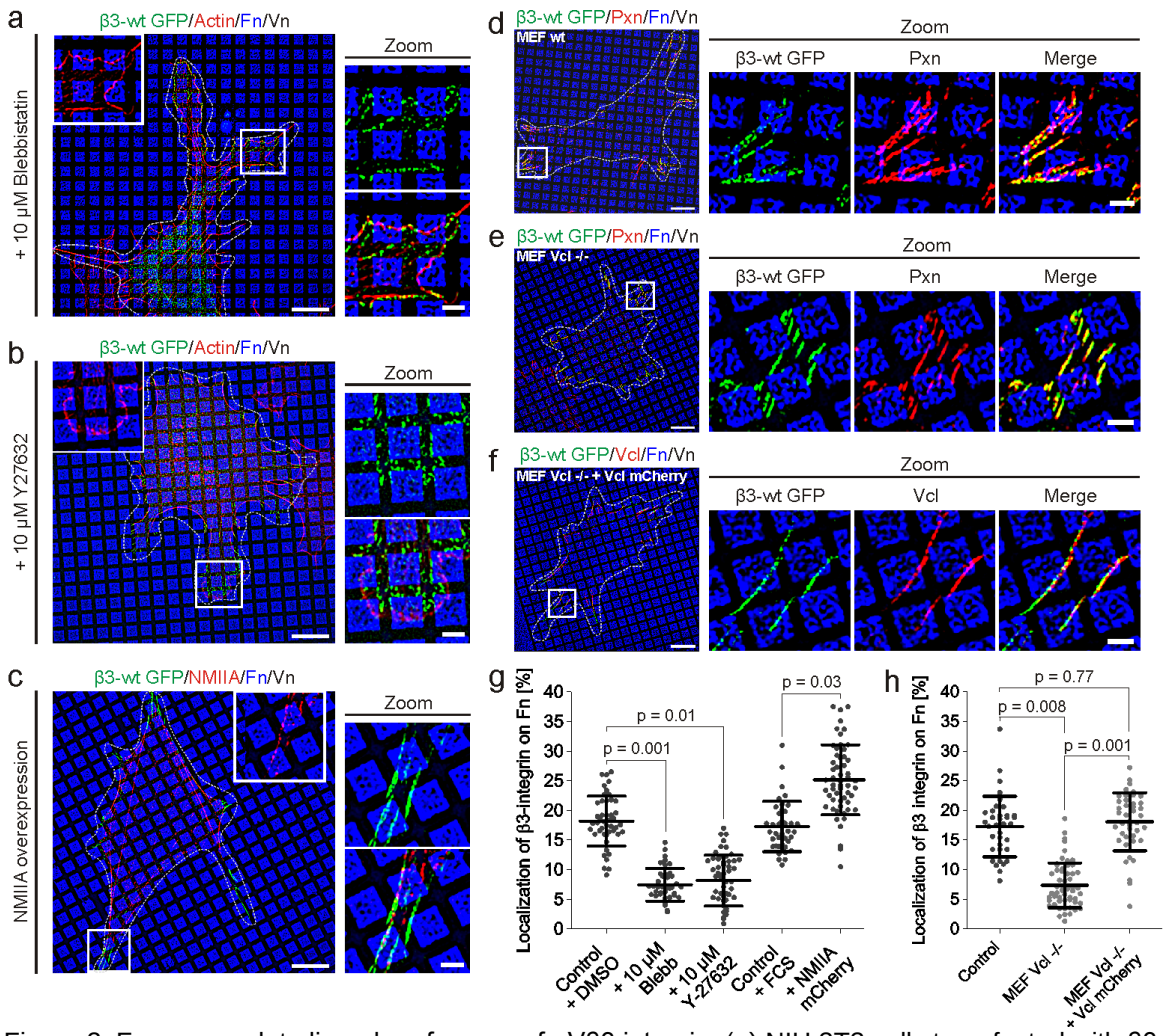

Figure 2: Forces regulate ligand preference of αVβ3 integrin. (**a**) NIH 3T3 cells transfected with β3-wt GFP integrin (green) were cultured on Fn/Vn substrates (Fn in blue) in the presence of blebbistatin and were stained after fixation for actin (red). (**b**) NIH 3T3 cells treated with Y27632. (**c**) NIH 3T3 cells transfected with β3-wt GFP integrin (green) and myosin IIA mApple (NMIIA; red) with serum (FCS) present in the medium. (**d**) MEF wt or (**e**) MEF vinculin knockout cells (MEF Vcl -/-) transfected with β3-wt GFP integrin (in green) and immunostained for paxillin (Pxn; red). (**f**) MEF Vcl -/- cells transfected with β3-wt GFP integrin (green) and Vcl mCherry (red). (**g**) Quantifications of colocalization of β3-wt GFP with Fn for cells treated as described in **a-c** (control + FCS: n = 66, N = 3; control + DMSO: n = 46, N = 3; + 10 µM blebbistatin: n = 40, N = 3; + 10 µM Y-27632: n = 54, N = 3; + NMIIA mCherry: n = 55, N = 3). Cells for "control + FCS" were treated as described in Fig. 1c except that they were cultured with FCS to allow proper comparison. (**h**) Quantifications of colocalization of β3-wt GFP with Fn for cells treated as described in **d-f** (control: n = 38, N = 3; MEF Vcl -/-: n = 57, N = 3; MEF Vcl -/- + Vcl mCherry: n = 42, N = 3). (**a-f**) All fluorescent images were acquired with SR-SIM. White dashed lines indicate the cell outline. Scale bar: 10 µm in overview images, 2 µm in zoom ins.

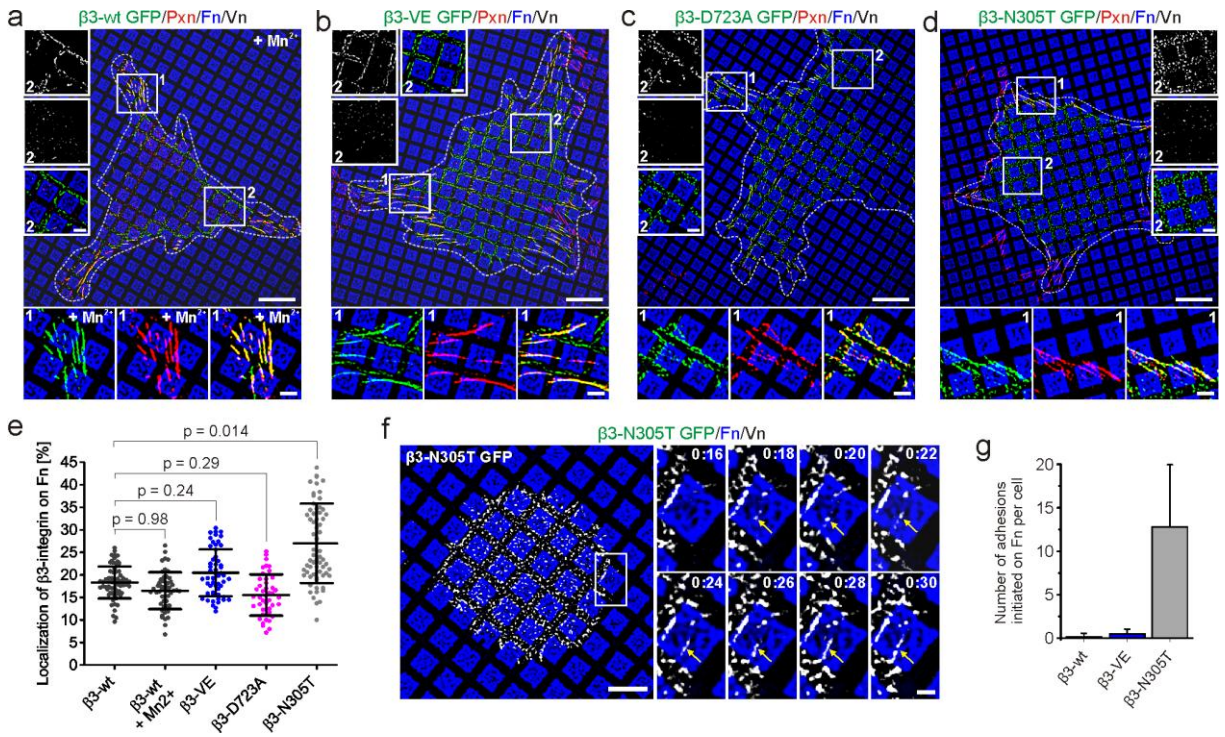

Figure 3: Hybrid domain swing-out is necessary for αVβ3 integrin binding to FN. (**a**) NIH 3T3 cell transfected with β3-wt GFP integrin (green). 1 mM Mn^{2+} was added to the medium 30 min before fixation. (**b**) NIH 3T3 cell transfected with β3-VE GFP integrin (green), or (**c**) for β3-D723A GFP integrin (green), or (**d**) for β3-N305T GFP integrin (green). All cells (**a-d**) were fixed and immunostained for paxillin (Pxn; red). Zoom-ins depict adhesions in the cellular periphery (1) or the cell center (2). (**e**) Quantifications of colocalization of β3-wt GFP with Fn for cells treated as described in **a-d**. Paxillin was used as a mask to exclude nascent αVβ3 integrin clusters in the cell center from analysis (β3-wt: replot of the data from Fig. 1d; β3-wt + Mn2+: n = 55, N = 3; β3-VE: n = 54, N = 3; β3-D723A: n = 43, N = 3; β3-N305T: n = 66, N = 4). (**f**) Live cell SR-SIM imaging of a NIH 3T3 cell transfected with β3-N305T GFP integrin (white) spreading on Fn/Vn substrates (Fn in blue). Yellow arrows indicate an αVβ3 integrin-mediated adhesion that initiated on Fn. (**g**) Number of αVβ3 integrin-mediated adhesions per cell that initiated on Fn for NIH 3T3 cells transfected with the indicated integrin (β3-wt is a replot of the data in Fig. 1f; β3-VE: six cells analyzed out of three independent experiments; β3-N305T: six cells analyzed out of four independent experiments). (**a-d, f**) Scale bars: overview images 10 µm, zoom-ins 2 µm. White dashed lines indicate the cell outline. Images acquired with SR-SIM.

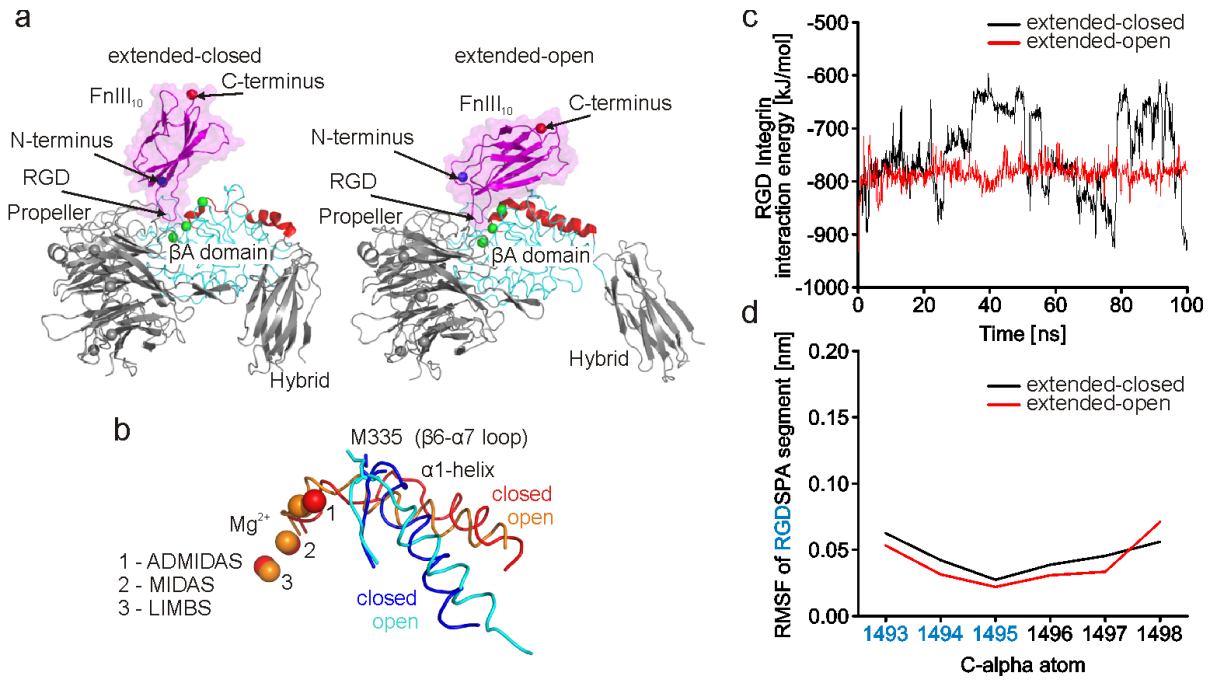

Figure 4: MD simulations confirm that Fn binds to extended-open αVβ3 integrin. (**a**) Snapshot of extended-closed and extended-open conformation of FnIII10-bound αVβ3 integrin of a molecular dynamics (MD) simulation. (**b**) Overlay of the conformations of α1-helix (residues 121 to 145) and β6-α7 loop in extended-closed (dark red and dark blue) and extended-open (orange and cyan) conformation with metal ions at the indicated coordination sites. Note the movement of the ADMIDAS ion away from M335 of the β6-α7 loop during headpiece opening. (**c**) Interaction energy between the RGD motif of FnIII10 and integrin over time of the MD simulation. (**d**) Root mean square fluctuation (RMSF) of the RGDSPA sequence of FnIII10 bound to integrin with blue highlighting the RGD amino acids.

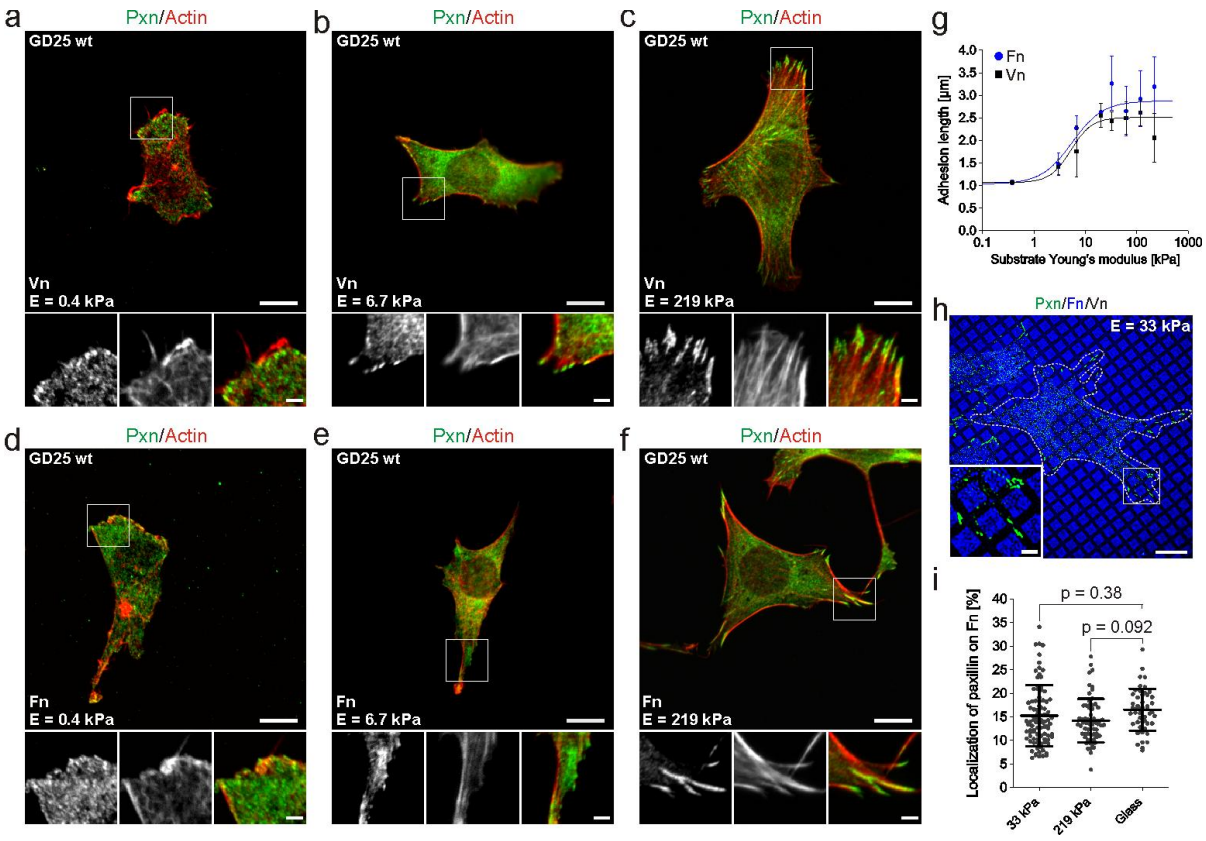

Figure 5: αVβ3 integrin mediates mechanotransduction and prefers Vn over a wide stiffness range. (**a-f**) GD25wt were cultured on elastic polyacrylamide gels of the indicated Young's modulus (E) and stained for paxillin (green) and actin (red). Cells were imaged with diffraction limited microscopy. Gels were coated homogeneously (**a-c**) with Vn or (**d-f**) with Fn. (**g**) Length of paxillin-stained adhesions (longest 25% only) was plotted against the Young's modulus for cells on Vn (black data points) or Fn (blue data points) revealing a mechanical switch for both ligands around 5 kPa (see Supplementary Table 1 for number of analyzed cells; N = 3 for all conditions). (**h**) Immunostained GD25wt cell (paxillin: green; Fn: blue) on a gel with a Young's modulus of E = 33 kPa functionalized with Fn/Vn patterns and imaged with SR-SIM. The zoom-in highlights the preferred localization of adhesions on Vn. White dashed line indicates cell outline. (**i**) Quantification of the colocalization of paxillin with Fn for cells grown on Fn/Vn pattern printed on glass (n = 36, N = 3), gels with E = 33 kPa (n = 93, N = 3), or gels with E = 219 kPa (n = 64, N = 3). (**a-f, h**) Scale bar: 10 µm in overviews, 2 µm in zoom-ins.

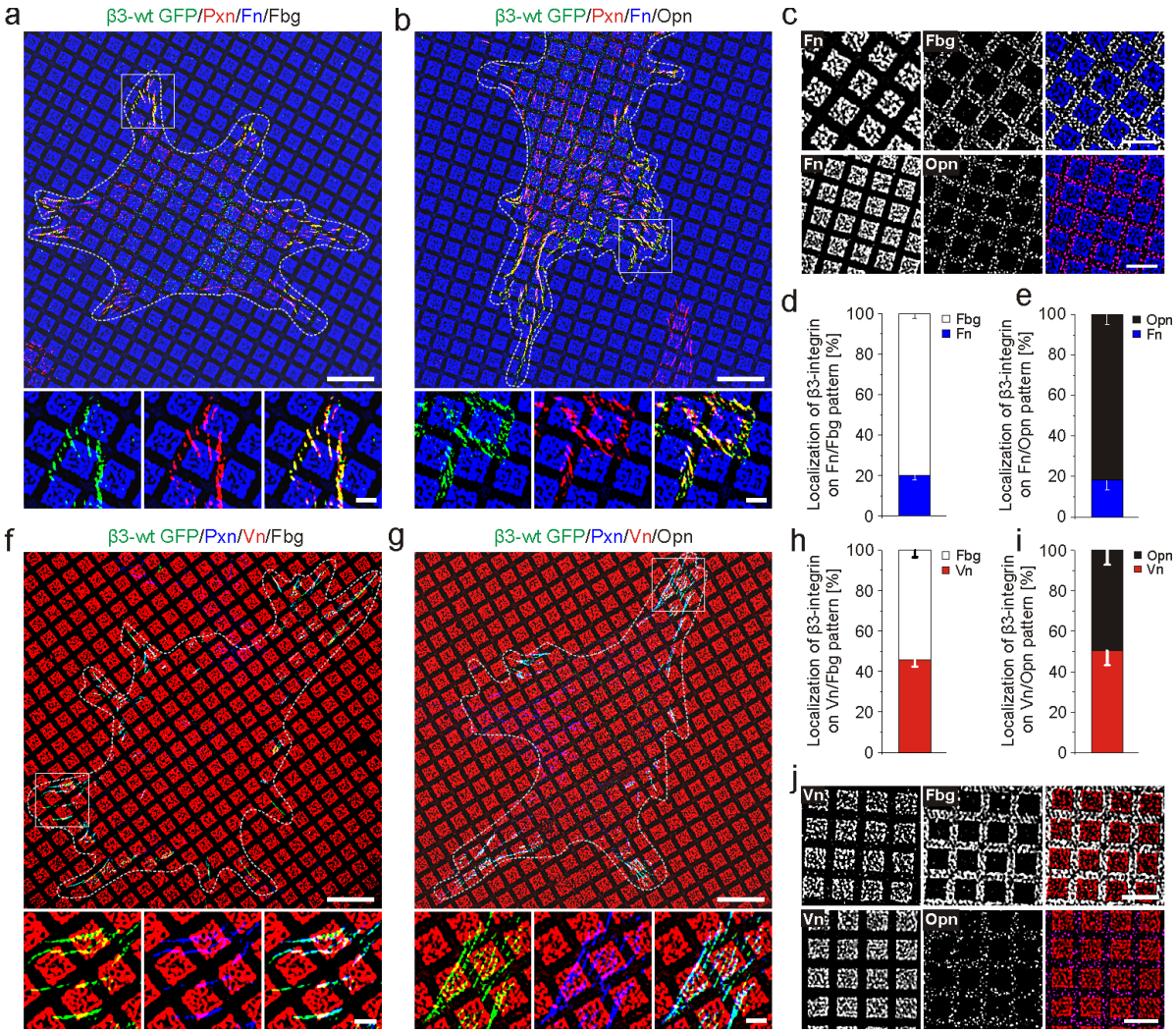

Figure 6: Vitronectin (Vn), osteopontin (Opn), and fibrinogen (Fbg) are high-affinity ligands for αVβ3 integrin. (**a**) Fn squares (blue) were stamped onto cover slips and the remaining area was backfilled with Fbg (black). NIH 3T3 cells transfected with β3-wt GFP integrin (green) cultured on Fn/Fbg substrates in the presence of 1% FCS and immunostained for paxillin (red). (**b**) Cell on a Fn/Opn pattern. (**c**) Staining of Fn/Fbg (Fn in blue; Fbg in white) and Fn/Opn (Fn in blue; Opn in magenta) patterns revealing successful protein separation. (**d**, **e**) Quantification of the colocalization of β3-wt GFP with indicated ECM proteins for cells cultured on Fn/Fbg (n = 69, N = 4) or Fn/Opn substrates (n = 53, N = 3). (**f**) Vn squares (red) were stamped on cover slips and the remaining area was backfilled with Fbg (black). NIH 3T3 cells transfected with β3-wt GFP integrin (green) cultured on Fn/Fbg substrates in presence of 1% FCS and immunostained for paxillin (blue). (**g**) Cell on a Vn/Opn pattern. (**h**, **i**) Quantification of the colocalization of β3-wt GFP with indicated ECM proteins for cells cultured on Vn/Fbg (n = 57, N = 3) or Vn/Opn substrates (n = 45, N = 3). (**j**) Staining of Vn/Fbg (Vn in red; Fbg in white) and Vn/Opn (Vn in red; Opn in magenta) patterns revealing successful protein separation. Scale bars: (**a**, **b**, **f**, **g**) 10 µm in the overview, 2 µm in the zoom in, (**c, j**) 5 µm. (**a**, **b**, **f**, **g**) White dashed lines indicate cell outline. All images acquired with SR-SIM.

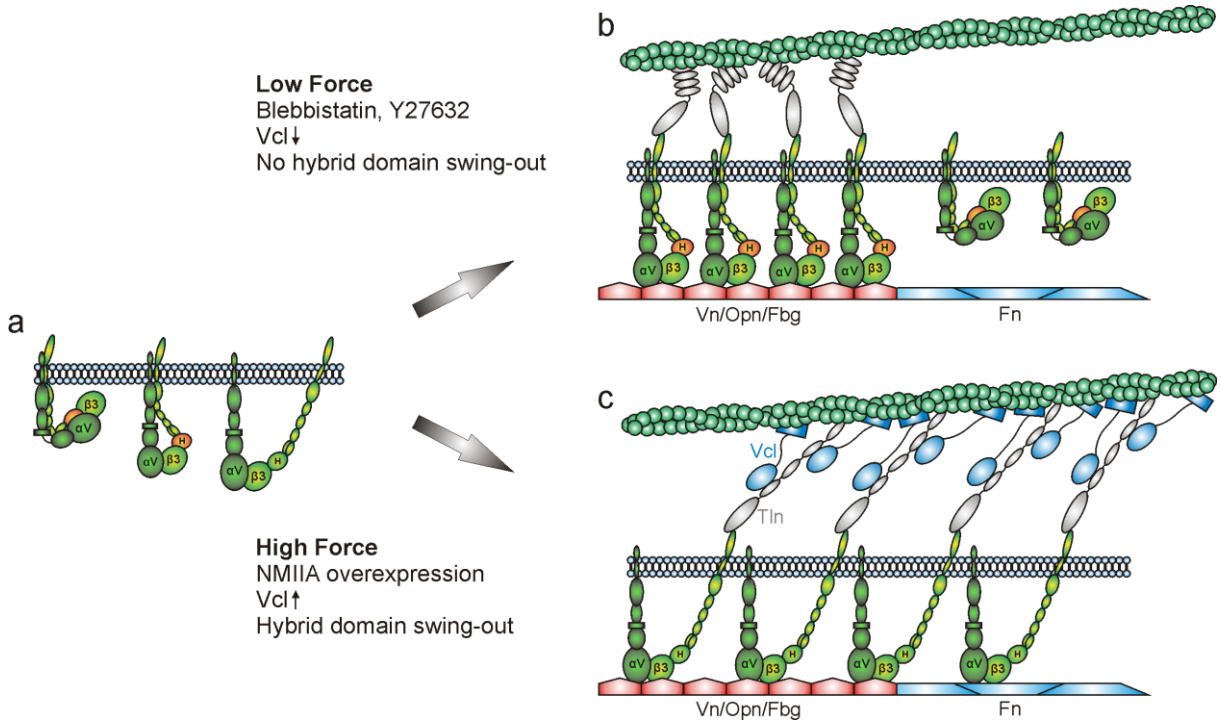

Figure 7: Model for the regulation of αVβ3 integrin by mechanical force and outside-in signaling. (**a**) Conformation of αVβ3 integrin in bent, extended-closed, and extended-open conformation (from left to right). Hybrid domain swing-out in the β3 subunit is coupled to the extended-open conformation indicated by the color change of the hybdrid domain from orange to green. (**b**) αVβ3 integrin in a low-force state (either caused by contractility inhibition or by missing vinculin (Vcl; simplified with head and tail region) recruitment to talin) favors binding to high-affinity ligands like Vn/Opn/Fbg. (**c**) In contrast, a high-force state of αVβ3 integrin (either caused by elevated myosin levels (NMIIA overexpression) or by vinculin binding to stretched talin (Tln; simplified structure with head domain and reduced number of rod domains)), favors the hybrid domain swing-out enabling Fn binding and in consequence a shift of αVβ3 integrins to Fn.

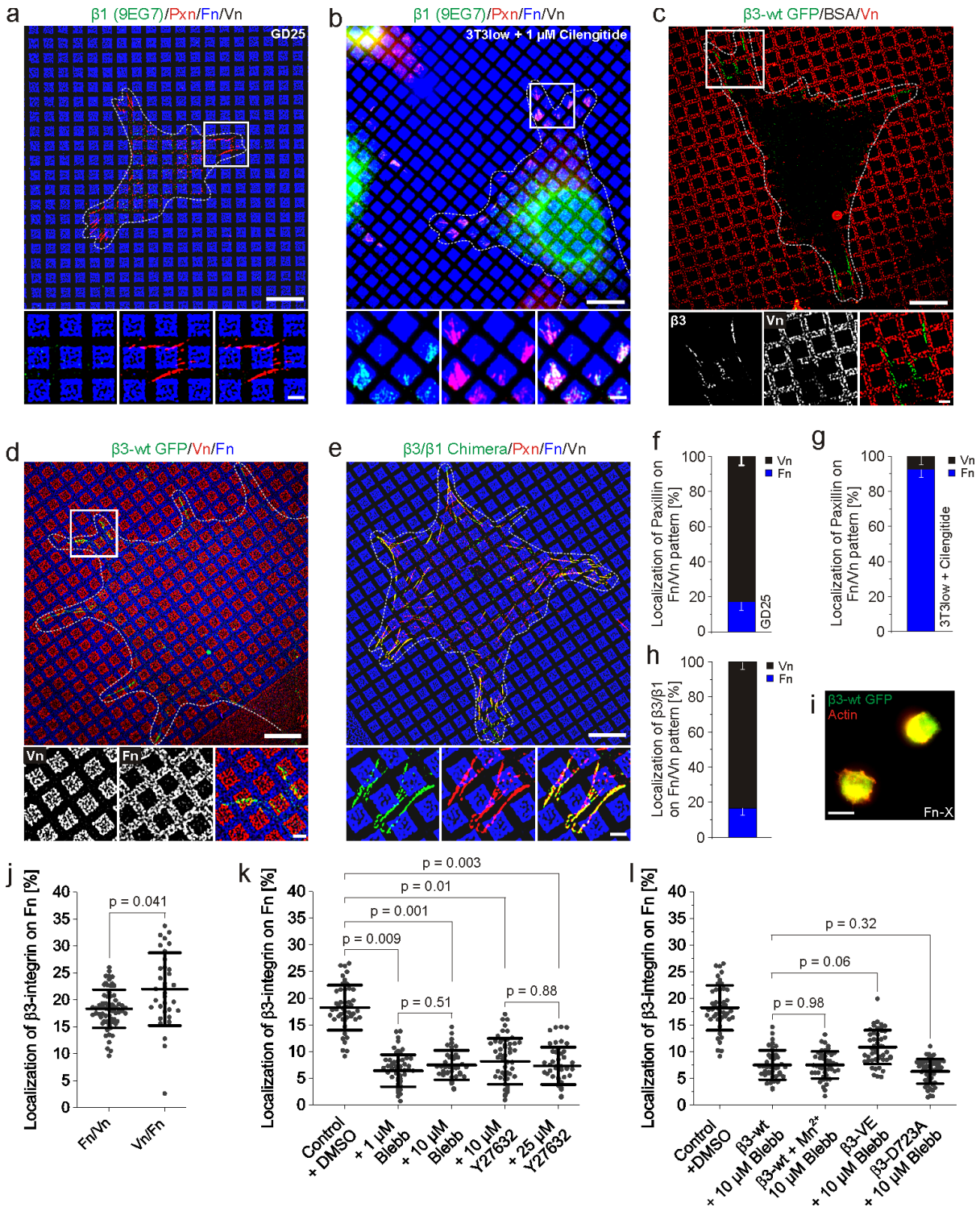

Supplementary Figure 1: (**a**) GD25 cells cultured on Fn/Vn substrates (Fn in blue) and immunostained for β1 integrin (green) and paxillin (red). GD25 cells express no β1 integrin (shown by the immunostaining for β1 integrin; left zoom in and merge with paxillin on the right). (**b**) NIH 3T3 cells cultured on Fn/Vn substrates (Fn in blue) and immunostained for β1 integrin (green) and paxillin (Pxn; red). Cilengitide, an αVβ3 integrin inhibitor, was added 30 min before fixation. Paxillin is restricted to Fn. (**c**) Bovine serum albumin (BSA) was stamped and backfilled with Vn (red; labeled by immunostaining). NIH 3T3 cells transfected with β3-wt GFP integrin were cultured on these substrates. Zoom-ins show that clustered αVβ3 integrin is not present on BSA. (**d**) Vn labeled with Alexa Fluor 568 (red) was stamped and then overlaid with Alexa Fluor 647 labeled Fn (blue). NIH 3T3 cells were transfected with β3-wt integrin (green) and cultured on these Vn/Fn substrates. (**e**) NIH 3T3 cells were transfected with a β3/β1 integrin chimera (green) with the extracellular part of β3 integrin and the transmembrane and cytoplasmic part of β1 integrin. These cells were cultured on Fn/Vn

substrates (Fn in blue) and immunostained for paxillin (red). (**f**) Quantification of paxillin colocalization with Fn in GD25wt cells treated as described in **a** (n = 36, N = 3). The same data set is used in Fig. 4g. (**g**) Quantification of paxillin colocalization with Fn in NIH3T3 cells treated as described in **b** (n = 27, N = 4). (**h**) Quantification of β3/β1 integrin chimera colocalization with Fn in NIH3T3 cells treated as described in **e** (n = 38, N = 3). (**i**) NIH 3T3 cells transfected with β3-wt GFP integrin cultured on heat-inactivated Fn (Fn-X) that was used together with native Fn during stamping (see Material & Methods). Cells are unable to spread and to cluster integrins on this substrate. (**j**) Quantification of β3 integrin colocalization with Fn in NIH3T3 cells treated as described in **d**. Category "Fn/Vn" is a replot of Fig. 1d (Vn/Fn: n = 38, N = 3). Please note that, besides a significant difference, β3-wt GFP preferentially localizes on Vn coated areas irrespective of the stamping procedure. (**k**) Quantification of β3 integrin colocalization with Fn in NIH3T3 cells transfected with β3-wt integrin and cultured on Fn/Vn substrates. Cells cultured in presence of blebbistatin or Y27632 at the indicated concentrations. Values of 10 µM inhibitor concentration and DMSO control are replotted from Fig. 2g (+ 1 µM Blebb: n = 51, N = 3; + 25 µM Y27632: n = 56, N = 3). (**l**) Quantification of β3 integrin colocalization for the indicated mutations with Fn in NIH3T3 cells transfected with β3-wt integrin and cultured on Fn/Vn substrates. 30 min before fixation blebbistatin (and Mn^{2+} where indicated) was added at the indicated concentrations. Values of DMSO control and "β3-wt +10 µM Blebb" are a replot of Fig. 2g (β3-VE+10 µM Blebb: n = 55, N = 3; β3-wt+Mn^{2+} +10 µM Blebb: n = 45, N = 3; β3-D723A+10 µM Blebb: n = 49, N = 3). (**a-e**) White dashed lines in overview images indicate cell outlines. Scale bar: 10 µm in the overview and 2 µm for the zoom-in. All fluorescent images except **b** were acquired with SR-SIM.

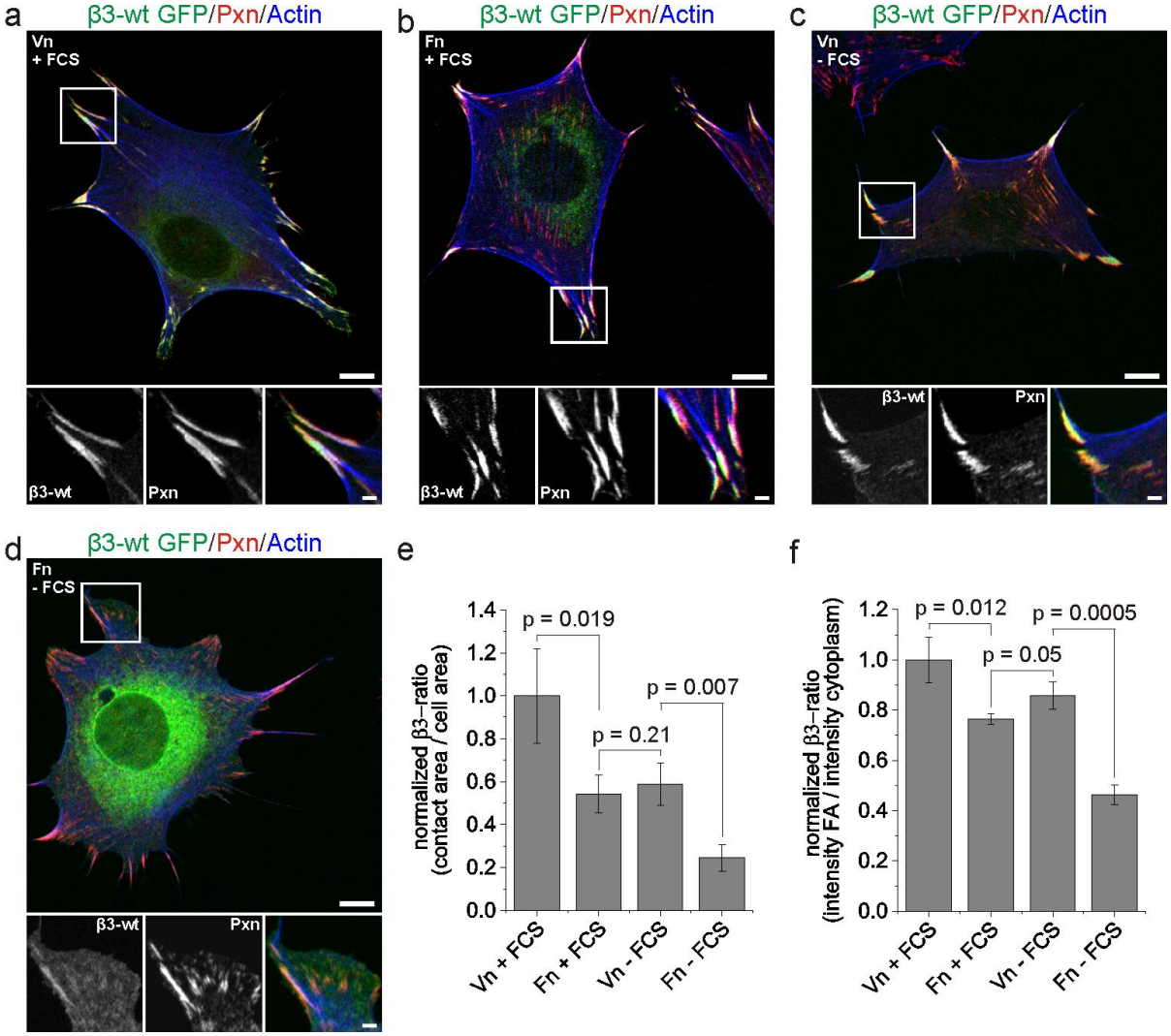

Supplementary Figure 2: αVβ3 integrin favors Vn compared to Fn on homogenous substrates. (**a-d**) NIH 3T3 cells transfected with β3-wt GFP (green) cultured on homogenously coated substrates (Vn or Fn as indicated) and stained for anti-paxillin (Pxn; red) and actin (blue). Throughout the experiment, fetal calf serum (FCS) was present in the medium at 10% v/v (+FCS) or not (-FCS). (**e**) Quantification of the size ratio of β3-wt GFP mediated cell-matrix adhesions compared to the cell area for the conditions described in **a-d**. Ratios are normalized to the ratio for Vn + FCS (Vn+FCS: n = 67, Fn+FCS: n = 69, Vn-FCS: n = 70, Fn-FCS: n = 67; N = 3 in all cases). (**f**) Quantification of the intensity ratio of β3-wt GFP mediated cell-matrix adhesions compared to the cytoplasm around the adhesions for the conditions described in **a-d**. Ratios are normalized to the ratio for Vn + FCS (same cells as in **e** were used for quantification; N = 3 in all cases). Scale bars: 10 µm in the overview, 2 µm in the zoom-ins.

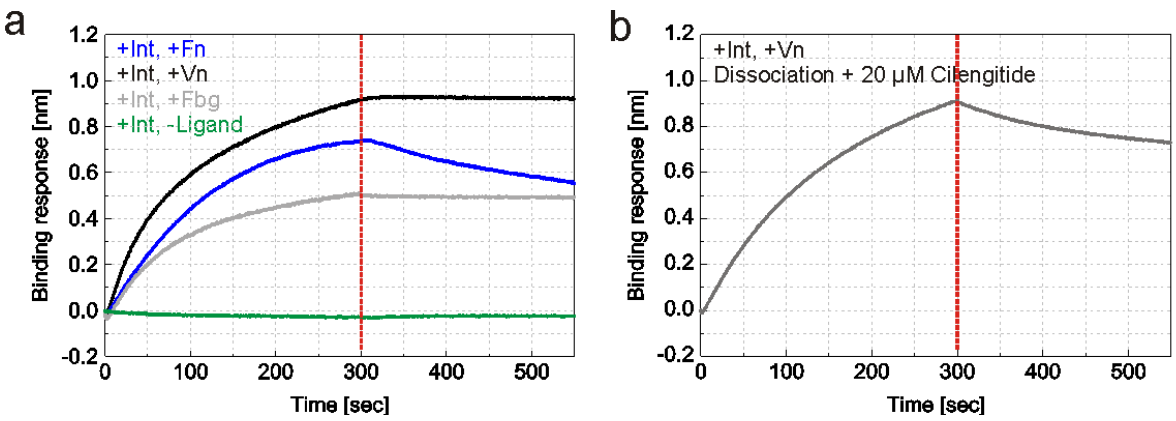

Supplementary Figure 3: (**a**) Association (0 – 300 s) and dissociation (300 – 550 s) curves for the interaction of the indicated ECM proteins with purified αVβ3 integrin. The measurements were performed with biolayer interferometry (representative curves from n = 9, N = 3 measurements for each condition). (**b**) Association and dissociation curve for Vn interaction with purified αVβ3 integrin. Cilengitide was present in the dissociation buffer at 20 µM concentration (representative curve from n = 9, N = 3 measurements).

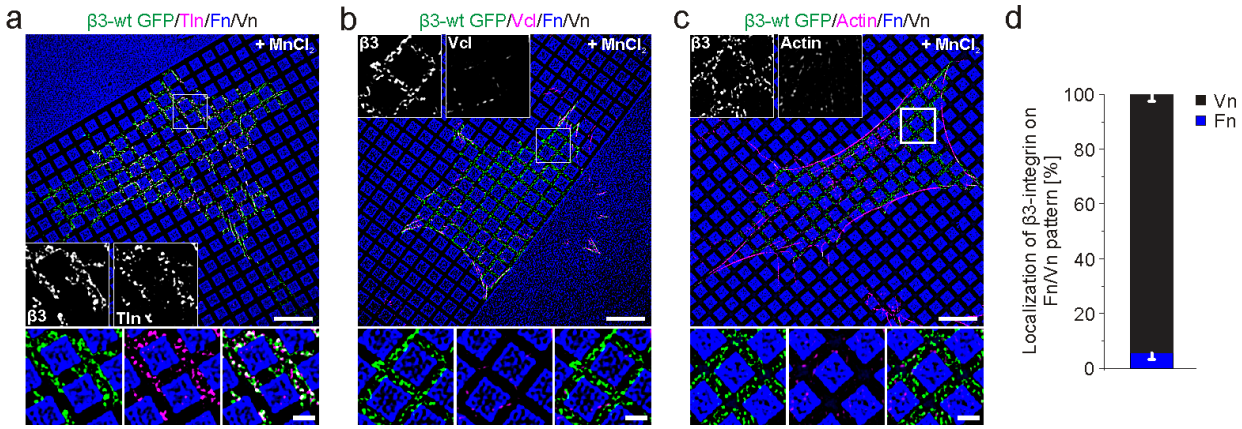

Supplementary Figure 4: (**a-c**) NIH 3T3 cells transfected with β3-wt GFP, cultured on Fn/Vn substrates and treated with 1mM Mn^{2+} 30 min before fixation. Additionally, cells were immunostained for (**a**) talin, (**b**) vinculin, or (**c**) for actin. (**d**) Quantification of β3-wt GFP in central areas of Mn^{2+} treated cells cultured as described in **a-c** but immunostained for paxillin. Only β3-wt GFP not colocalizing with paxillin was used for analysis to ensure exclusive measurement of nascent integrin clusters (n = 42; N = 3). (**a-c**) Scale bars: 10 µm in the overview, 2 µm in the zoom-ins.

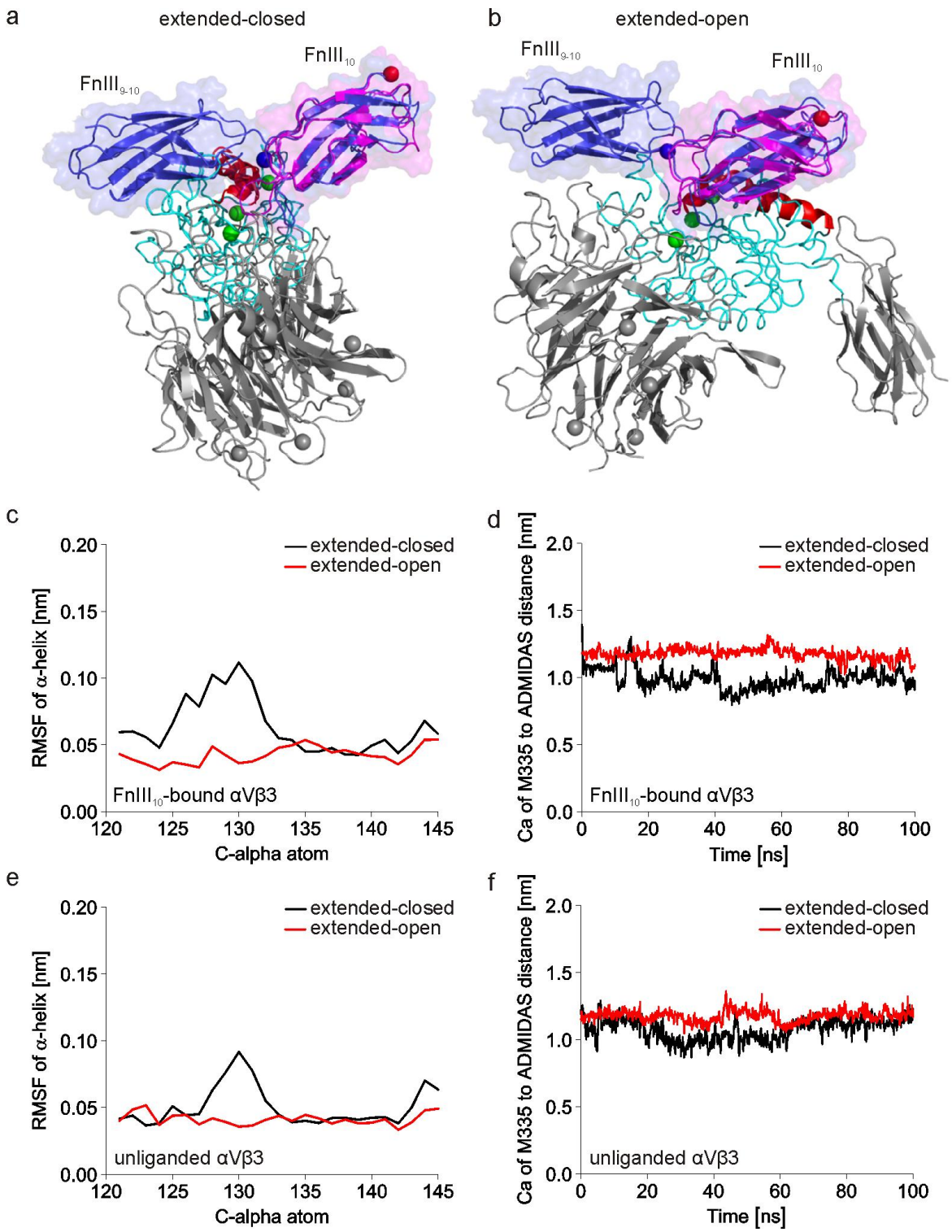

Supplementary Figure 5: Overlay of (**a**) extended-closed and (**b**) extended-open conformation from Fig. 4a with a Fn structure consisting of 9th and 10th domain of full-length Fn (FnIII9-10; blue). Please note steric clashes for the extended-closed conformation. Loops of the βA domain of β3 integrin (cyan) overlap with the 9th domain of Fn. This is not the case for the extended-open conformation. (**c, e**) Root mean square fluctuation (RMSF) against indicated C-alpha atoms of α1-helix in (**c**) FnIII10-bound and (**e**) unliganded state of integrin. (**d, f**) The distance between Cα atom of M335 at β6-α7 loop and ADMIDAS ion plotted against the time course of the MD simulation in (**d**) Fn10-bound and (**f**) unliganded state of integrin.

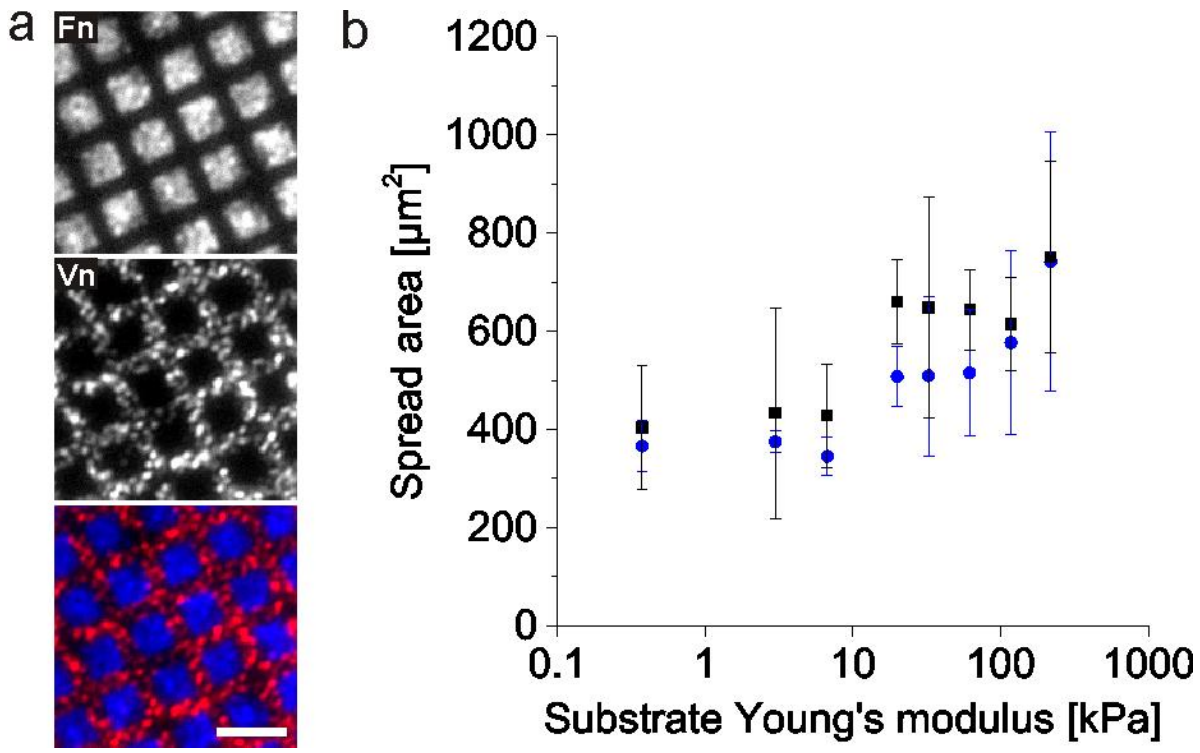

Supplementary Figure 6: (**a**) Protein separation of Fn/Vn patterns tested after transfer of the pattern to polyacrylamide gels by immunostaining for Fn (blue) and Vn (red). (**b**) For cells analyzed in Fig. 5g, cell size was quantified and plotted against the Young's modulus of the gel substrates. Black data points represent Vn coated, blue data points Fn coated elastic gels.

Supplementary Videos

Supplementary Video 1: NIH 3T3 cell expressing β3-wt GFP (green) was monitored during spreading on Fn/Vn substrate (Fn in blue) with live-cell SR-SIM with 1 frame per minute. See also Fig. 1g.

Supplementary Video 2: Zoom-in of Supplementary Video 1.

Supplementary Video 3: NIH 3T3 cell expressing β3-N305T GFP (white) was monitored during spreading on Fn/Vn substrate (Fn in blue) with live-cell SR-SIM with 1 frame per minute. See also Fig. 3f.

Supplementary Video 4: Zoom-in of Supplementary Video 3.

Supplementary Video 5: NIH 3T3 cell expressing β3-VE GFP (white) was monitored during spreading on Fn/Vn substrate (Fn in blue) with live-cell SR-SIM with 1 frame per minute.

Supplementary Video 6: Zoom-in of Supplementary Video 5.

Supplementary Table 1: Polyacrylamide gel rigidities measured with AFM. Number of analyzed cells refers to Fig. 4g and Supplementary Fig. 5b.

Young's module [Pa] **mean ± standard deviation**	**acrylamide, final concentration [%]**	**bisacrylamide, final concentration [%]**	**analyzed cells on Fn**	**analyzed cells on Vn**
0.4 ± 0.08	4	0.03	22	22
3.0 ± 0.98	5.5	0.04	25	33
6.7 ± 1.95	7.46	0.04	25	31
20.1 ± 4.87	7.49	0.10	29	40
32.6 ± 9.38	7.52	0.16	33	39
61.7 ± 27.03	12	0.15	32	37
117.3 ± 20.29	12	0.2	39	42
218.7 ± 44.39	12	0.3	31	33

Methods:

Cell culture, constructs, and transfection

NIH 3T3 cells used in this study are a subclone of NIH3T3 cells that were FACS sorted for low expression of endogenous β3-integrin as described previously (Pinon et al., 2014). Vinculin-knockout mouse embryonic fibroblasts (MEF Vcl -/-) and MEF wt were kindly provided by W. H. Ziegler (Mierke et al., 2010). GD25wt cells were kindly provided by R. Fässler (Wennerberg et al., 1996). All cells were grown at 37°C with 5% CO_2 in DMEM (ThermoFischer) supplemented with 10% FCS (Hyclone), and passaged 2-3 times a week, or upon reaching confluency. Transfections were carried out with Lipofectamine 2000 (ThermoFischer) according to manufacturer's instructions. 6 h after transfection, cells were cultured in complete medium for 48h before detachment. cDNA encoding full-length mouse β3-wt GFP integrin expressed in a cytomegalovirus promoter-driven pcDNA3/EGFP vector has been previously described (Ballestrem et al., 2001). β3-VE GFP (Pinon et al., 2014), β3-D723A GFP (Ballestrem et al., 2001), and β3-N305T GFP (Ballestrem et al., 2001) were derived by substitution from the β3-wt GFP integrin construct mentioned before and as described in the indicated publications. Vinculin mCherry was a gift from Christoph Ballestrem (Manchester, UK) and mApple-MyosinIIA-C-18 was a gift from Michael Davidson (Addgene plasmid # 54929).

Antibodies and chemicals

Inhibition experiments were performed with blebbistatin (Sigma-Aldrich), with the ROCK inhibitor Y27632 (Sigma-Aldrich), or with the αVβ3 integrin inhibitor cilengitide (Sellekchem) at concentrations as indicated. Cells were fixed for subsequent immunostaining with 4% PFA (Sigma-Aldrich) in PBS. Reagents used for immunostaining were monoclonal mouse antibodies for paxillin (clone 349/Paxillin, BD Biosciences, # 610052), talin (clone 8d4, Sigma-Aldrich, #T3287), vinculin (clone hVIN-1, abcam, #ab11194), vitronectin (clone VIT-2, IgM, Sigma-Aldrich, #V7881) or polyclonal rabbit antibodies for fibronectin (Sigma-Aldrich, #F3648) or osteopontin (GeneTex, #GTX37582). β1-integrin was stained with a monoclonal rat antibody (clone 9EG7, BD Biosciences, # 553715). After primary antibody staining, samples were washed and incubated with antibodies against mouse labeled with Cy3 (Jackson Immunoresearch, #115-165-146), against rabbit labeled with Alexa Fluor 488 (ThermoFischer, #A11070), or with phalloidin coupled to Alexa Fluor 568 (ThermoFischer, #A12380). To visualize anti-Vn staining, secondary antibodies against IgM labeled with Cy3 were used (Dianova, #115-166-075). Primary rat antibodies were visualized with preadsorbed, Alexa Fluor 488 labeled secondary antibodies (ThermoFischer, #A11006) and primary mouse antibodies were in this case visualized with preadsorbed, Cy3 labeled antibodies (Dianova, #111-165-144) to avoid cross-reactivity of secondary antibodies. Direct labeling of Fn, Fbg, and Vn was performed according to manufacturer's protocol with Alexa Fluor 568 (ThermoFischer, # A10238) or Alexa Fluor 647 (ThermoFischer, #A20173).

Microcontact printing

Silicone stamps for microcontact printing of differential substrates were produced as previously described (Lehnert et al., 2004). Binary choice susbtrates were produced with human plasma fibronectin (Sigma-Aldrich, #F2006 or Millipore, #FC010), human plasma vitronectin (Sigma-Aldrich, #V8379), recombinant human vitronectin (Sigma-Aldrich, #SRP3186), native human fibrinogen (Bio-Rad, #4440-8604), or with osteopontin from bovine milk (Sigma-Aldrich, #O3514). Silicone stamps were incubated for 10 min with a solution of 5 µg/ml Fn and 45 µg/ml heat-inactivated Fn in PBS (see Supplementary Fig. 1i). Alexa Fluor 647 labeled Fn was added to visualize the Fn pattern. After nitrogen drying, the stamp was pressed onto a glass cover slip for 10 min before it was released. Next, the pattern was covered with Vn at a concentration of 5 µg/ml in PBS for 1 hour at room temperature. Heat-inactivated Fn was produced by heating Fn for 30 min to 90°C and was added to block Vn adsorption in the stamped area. Cells do not spread on heat-inactivated Fn (Supplementary Fig. 1i). For other binary choice substrates than Fn/Vn, a total concentration of 50 µg/ml of the stamped protein, and 5 µg/ml of the protein for backfilling was used. All other steps were performed as described. After the final incubation step, patterns were washed with PBS and used directly for cell seeding. Cell detachment from culture flasks was stopped with trypsin inhibitor (Sigma-Aldrich) and cells were seeded in DMEM without FCS if not stated otherwise.

Polyacrylamide gels

Established protocols (Kandow et al., 2007, Pinon et al., 2014, Plotnikov et al., 2014) were adapted to gain polyacrylamide gels of different Young's modulus (stiffness) with homogeneous or with structured ECM. Gels were produced on activated cover slips. Therefore, glass cover slips were cleaned first with propanol and second for 10 min in a plasma cleaner (Technics Plasma GmbH, Germany). This was followed by a silanization (1 h at room temperature, 1 mM 3-(Trimethoxysilyl)propyl methacrylate

(Sigma-Aldrich) in toluene). After incubation, cover slips were washed in ddH_2O and dried with nitrogen. On these cover slips, 60 µl of a mixture of degassed acrylamide, bisacrylamide (both Bio-Rad), tetramethylethylenediamine, and ammonium persulfate (TEMED and APS; Sigma-Aldrich) was pipetted with final concentrations of 0.5% APS, 0.1% TEMED, and as mentioned in Supplementary Table 1. This solution was covered with 10 µl of 1% w/v of Acrylic acid *N*-hydroxysuccinimide ester (NHS acrylate; Sigma-Aldrich) in toluene. Finally, the solution was covered with a cover slip of 18 mm diameter that was either functionalized with a Fn/Vn pattern prepared as described before or that was coated with a 50 µg/ml solution of Fn or Vn for 1h at room temperature. This top cover slip was dried with nitrogen before it was applied to the gel solution. After polymerization, the top cover slip was removed and the gel was covered with PBS. Gel substrates were used directly for cell seeding or were stored overnight at 4°C before cell seeding.
Stiffness of polyacrylamide gels was measured as previously described (Elosegui-Artola et al., 2016). Measurements were performed with the atomic force microscope described below. Silicon nitride pyramidal tips with a nominal spring constant of k = 0.01-0.03 Nm^{-1} were used (MLCT, Bruker). An effective half-angle of 20° was used for calculation. For each stiffness, 3 gels from 3 independent batches were measured by probing 5 positions in the center of the gel with 5 repetitive measurements. The Hertz model equation for pyramidal tips was fitted to the force-displacement curves.

Microscopy
SR-SIM imaging was performed on a non-serial Zeiss Elyra PS.1 microscope with a 63x/1.4NA oil immersion objective and an Andor iXon EMCCD camera. The grid for SR-SIM was rotated three times and shifted five times leading to 15 frames raw data out of which a final SR-SIM image was calculated with the structured illumination package of ZEN software (Zeiss). Values for calculation were selected for best resolution without causing image artifacts. Channels were aligned by using a correction file that was generated by measuring channel misalignment of fluorescent tetraspecs (ThermoFischer, #T7280). Images of cells on homogeneous polyacrylamide gels were taken using the ApoTome module on a Zeiss AxioimagerZ1 microscope to achieve optical sectioning. A 63x/1.4NA oil immersion objective and a Zeiss AxioCam MRm were used. For SR-SIM live cell microscopy, the incubation chamber was heated to 37°C and cells were imaged every minute. During imaging, cells were cultured in imaging medium (F12 + 25 mM HEPES + 200 mM L-glutamine + 1% penicillin/streptomycin + 10% FCS, pH 7.2). SIM raw data images were processed as described above.

Atomic Force Microscopy
To prepare adhesion substrates for directly comparative adhesion force spectroscopy, adjacent areas on a Fluorodish 35 (WPI) glass bottom dish were coated with 50 µg/ml BSA (to provide low adhesion for cell capture, see below), 50 µg/ml Fn, or 5 µg/ml Vn solutions and incubated for 1h. Substrates were subsequently rinsed five times with PBS and transferred to CO_2-independent Medium (ThermoFischer). Prior to SCFS experiments, GD25wt cells were transferred to CO_2-independent Medium for 1 h and then trypsinized. Trypsin was subsequently inactivated by adding soybean trypsin inhibitor (Sigma-Aldrich). After centrifugation, the supernatant was removed, and cells were again resuspended in CO_2-independent Medium. SCFS experiments were performed using a CellHesion 200 atomic force microscope (JPK) featuring an extended vertical range of 100 µm. All measurements were performed at 37ºC using a temperature-controlled sample chamber (BioCell from JPK) and tipless 205 µm long V-shaped cantilevers with a nominal spring constant of 0.06 N/m (NP-O from Veeco). To facilitate cell capture, plasma-cleaned cantilevers were functionalized with concanavalin A. After calibrating the sensitivity of the optical lever system and determining the spring constant, cells were pipetted into the sample chamber. A single cell was captured above the BSA coated area by pressing the functionalized cantilever onto the cell with a contact force of 500 pN for 3 s and elevating the cantilever subsequently. To measure cell detachment forces, the cantilever was lowered at a constant speed of 5 µm/s until the cell made contact with the substrate and a preset force of 1.5 nN was reached. Afterwards, the cantilever was held at a constant height for the preset contact time until the cantilever was elevated 80 µm above the substrate surface. Each cell was tested alternatingly on Fn and Vn surfaces (typically 10 force cycle repetitions for each contact time) to determine the differential adhesion strength to both ligands. In total, 8 different cells were tested. Detachment forces were analyzed using the JPK image processing software. From the collected force-distance curves, the maximum detachment forces (maximum cantilever deflection) were determined and plotted as mean ± SD using OriginPro 8.1G. Statistical significance of experiments was tested with a Wilcoxon-based Mann-Whitney U-test using InStat.

Image Analysis
Colocalization, cell area, and adhesion length were analyzed with the Fiji software package (Schindelin et al., 2015). A threshold was applied to the intensity of the corresponding fluorescent

channel and the area or the length of individual integrin-mediated adhesions was measured with plugins included in Fiji. Colocalization to Fn was quantified by measuring Mander's coefficient of thresholded images by using the Fiji plugin JACoP (Bolte and Cordelieres, 2006). The location of adhesion initiation on Fn/Vn substrates was defined by analyzing SR-SIM live cell movies. The fluorescent channel of the integrin staining was analyzed while the Fn channel was hidden. Integrin clusters visible for at least two subsequent time frames were marked with an ellipse in the ZEN imaging software throughout the movie. Afterwards, the Fn channel was uncovered, and the positions of all ellipses were counted with respect to FN squares or Vn surrounding the squares. If an integrin cluster initiated at the border of a square with contact to Fn and Vn, it was counted for the category Fn/Vn.

Biolayer interferometry measurement

Dissociation constants of αVβ3 integrin binding to different ECM proteins were measured using the BLItz biolayer interferometer (Pall ForteBio). All steps during real-time measurements were performed at room temperature in the same buffer conditions (20 mM Tris, 150 mM NaCl, pH 7.4, 1mM $MgCl_2$, 1 mM $CaCl_2$, 0.02% Tween20, 0.1% BSA). Pre-hydrated (10 minutes in integrin buffer) Ni-NTA biosensors (Pall ForteBio) were loaded with 50 µg/ml His-tagged human recombinant αVβ3 integrin (RnD Systems, #3050-AV) following an association phase with 150 µg/ml ECM protein and a dissociation phase (baseline – 45s; loading – 180s; baseline – 45s; association – 300s, dissociation – 300s). Binding curves were corrected for a reference sample, and K_D values were calculated from association rate constants, and dissociation rate constants derived by software from local curve fits corrected for start of association and dissociation. In control experiments, 20 µM cilengitide was added to the integrin buffer during dissociation phase (Supplementary Fig. 4b). A 10 s adjustment step was included.

Molecular Dynamic Simulation

In simulations, we used the structure of FnIII10–bound integrin in extended-closed and extended-open form including propeller, βA, and hybrid domains. Crystal structure of αVβ3 integrin from RCSB Protein Data Bank (ID: 4MMX) was used as a model for the extended-closed integrin. Structure of the extended-open form was prepared by superimposition of βA and hybrid domains from the crystal structure of open αIIbβ3 integrin (ID: 3FCU). Systems containing unliganded αVβ3 were prepared by removing FnIII10 from initial structure. MD simulations were performed using Gromacs ver 2016.1 (Van Der Spoel et al., 2005) at the Sisu supercomputer, CSC, Finland. The CHARMM27 force field (Bjelkmar et al., 2010) and explicit TIP3P water model (Jorgensen and Madura, 1983) in 0.15 M KCL neutral solution were used. Energy minimization of the system was performed in 25 000 steps using steepest descent algorithm. The system was equilibrated in three phases using harmonic position restraints on all heavy atoms of protein. The first phase of equilibration was performed with NVT ensemble for 100 ps using the Berendsen weak coupling algorithm (Berendsen et al., 1984) to control the temperature of the system at 100 K. Integration time step of 2 fs was used in all the simulations. Following NVT, the system is linearly heated from 100 to 310 K over 1 ns using an NPT ensemble at 1 atm of pressure. During this process, the Berendsen algorithm was used to control both temperature and pressure. For the final phase of equilibration and for all subsequent simulations, an NPT ensemble was maintained at 310 K, using V-rescale algorithm (Bussi et al., 2007), and 1 atm as implemented in Gromacs 2016.1. Temperature coupling was applied separately for protein and solution parts. Preparation of structures and analysis was performed using PyMOL 1.7. Interaction energy, which was calculated to evaluate FNIII10 RGD–integrin interactions, is a sum of Lennard-Jones and Coulomb energies.

Statistics

If not stated otherwise, reported values in bar charts are calculated as mean and error bars are representing standard deviation of the mean. In box plots, upper and lower bar indicate standard deviation and the middle bar indicates the mean. Statistical comparisons are calculated with two-tailed Student's t-test based on the number of independent experiments. For adhesion force measured with AFM, statistical significance of experiments was tested with a Wilcoxon-based Mann-Whitney U-test using InStat. All experiments were reproducible and were carried out as independent experiments as often as indicated in the figure legends.

References:

ARNAOUT, M. A., GOODMAN, S. L. & XIONG, J. P. 2007. Structure and mechanics of integrin-based cell adhesion. *Curr Opin Cell Biol,* 19**,** 495-507.

ATTIEH, Y., CLARK, A. G., GRASS, C., RICHON, S., POCARD, M., MARIANI, P., ELKHATIB, N., BETZ, T., GURCHENKOV, B. & VIGNJEVIC, D. M. 2017. Cancer-associated fibroblasts lead tumor invasion through integrin-beta3-dependent fibronectin assembly. *J Cell Biol*.

BALABAN, N. Q., SCHWARZ, U. S., RIVELINE, D., GOICHBERG, P., TZUR, G., SABANAY, I., MAHALU, D., SAFRAN, S., BERSHADSKY, A., ADDADI, L. & GEIGER, B. 2001. Force and focal adhesion assembly: a close relationship studied using elastic micropatterned substrates. *Nat Cell Biol,* 3**,** 466-72.

BALCIOGLU, H. E., VAN HOORN, H., DONATO, D. M., SCHMIDT, T. & DANEN, E. H. 2015. The integrin expression profile modulates orientation and dynamics of force transmission at cell-matrix adhesions. *J Cell Sci,* 128**,** 1316-26.

BALLESTREM, C., HINZ, B., IMHOF, B. A. & WEHRLE-HALLER, B. 2001. Marching at the front and dragging behind: differential alphaVbeta3-integrin turnover regulates focal adhesion behavior. *J Cell Biol,* 155**,** 1319-32.

BERENDSEN, H. J. C., POSTMA, J. P. M., GUNSTEREN, W. F. V., DINOLA, A. & HAAK, J. R. 1984. Molecular dynamics with coupling to an external bath. *The Journal of Chemical Physics,* 81**,** 3684-3690.

BJELKMAR, P., LARSSON, P., CUENDET, M. A., HESS, B. & LINDAHL, E. 2010. Implementation of the CHARMM Force Field in GROMACS: Analysis of Protein Stability Effects from Correction Maps, Virtual Interaction Sites, and Water Models. *J Chem Theory Comput,* 6**,** 459-66.

BOLTE, S. & CORDELIERES, F. P. 2006. A guided tour into subcellular colocalization analysis in light microscopy. *J Microsc,* 224**,** 213-32.

BUSSI, G., DONADIO, D. & PARRINELLO, M. 2007. Canonical sampling through velocity rescaling. *J Chem Phys,* 126**,** 014101.

CAMPBELL, I. D. & HUMPHRIES, M. J. 2011. Integrin structure, activation, and interactions. *Cold Spring Harb Perspect Biol,* 3.

CAO, L., NICOSIA, J., LAROUCHE, J., ZHANG, Y., BACHMAN, H., BROWN, A. C., HOLMGREN, L. & BARKER, T. H. 2017. Detection of an Integrin-Binding Mechanoswitch within Fibronectin during Tissue Formation and Fibrosis. *ACS Nano,* 11**,** 7110-7117.

CHOI, C. K., VICENTE-MANZANARES, M., ZARENO, J., WHITMORE, L. A., MOGILNER, A. & HORWITZ, A. R. 2008. Actin and alpha-actinin orchestrate the assembly and maturation of nascent adhesions in a myosin II motor-independent manner. *Nat Cell Biol,* 10**,** 1039-50.

CIOBANASU, C., FAIVRE, B. & LE CLAINCHE, C. 2014. Actomyosin-dependent formation of the mechanosensitive talin-vinculin complex reinforces actin anchoring. *Nat Commun,* 5**,** 3095.

CLUZEL, C., SALTEL, F., LUSSI, J., PAULHE, F., IMHOF, B. A. & WEHRLE-HALLER, B. 2005. The mechanisms and dynamics of (alpha)v(beta)3 integrin clustering in living cells. *J Cell Biol,* 171**,** 383-92.

DANEN, E. H., SONNEVELD, P., BRAKEBUSCH, C., FASSLER, R. & SONNENBERG, A. 2002. The fibronectin-binding integrins alpha5beta1 and alphavbeta3 differentially modulate RhoA-GTP loading, organization of cell matrix adhesions, and fibronectin fibrillogenesis. *J Cell Biol,* 159**,** 1071-86.

DAO, L., WEILAND, U., HAUSER, M., NAZARENKO, I., KALT, H., BASTMEYER, M. & FRANZ, C. M. 2012. Revealing non-genetic adhesive variations in clonal populations by comparative single-cell force spectroscopy. *Exp Cell Res,* 318**,** 2155-67.

DONG, X., ZHAO, B., IACOB, R. E., ZHU, J., KOKSAL, A. C., LU, C., ENGEN, J. R. & SPRINGER, T. A. 2017. Force interacts with macromolecular structure in activation of TGF-beta. *Nature,* 542**,** 55-59.

ELOSEGUI-ARTOLA, A., ORIA, R., CHEN, Y., KOSMALSKA, A., PEREZ-GONZALEZ, C., CASTRO, N., ZHU, C., TREPAT, X. & ROCA-CUSACHS, P. 2016. Mechanical regulation of a molecular clutch defines force transmission and transduction in response to matrix rigidity. *Nat Cell Biol,* 18**,** 540-8.

ENG, E. T., SMAGGHE, B. J., WALZ, T. & SPRINGER, T. A. 2011. Intact alphaIIbbeta3 integrin is extended after activation as measured by solution X-ray scattering and electron microscopy. *J Biol Chem,* 286**,** 35218-26.

ERDOGAN, B., AO, M., WHITE, L. M., MEANS, A. L., BREWER, B. M., YANG, L., WASHINGTON, M. K., SHI, C., FRANCO, O. E., WEAVER, A. M., HAYWARD, S. W., LI, D. & WEBB, D. J. 2017. Cancer-associated fibroblasts promote directional cancer cell migration by aligning fibronectin. *J Cell Biol*.

HUMPHRIES, J. D., BYRON, A. & HUMPHRIES, M. J. 2006. Integrin ligands at a glance. *J Cell Sci,* 119**,** 3901-3.

HUMPHRIES, J. D., WANG, P., STREULI, C., GEIGER, B., HUMPHRIES, M. J. & BALLESTREM, C. 2007. Vinculin controls focal adhesion formation by direct interactions with talin and actin. *J Cell Biol,* 179**,** 1043-57.

HYNES, R. O. 2002. Integrins: bidirectional, allosteric signaling machines. *Cell,* 110**,** 673-87.

HYTONEN, V. P. & WEHRLE-HALLER, B. 2016. Mechanosensing in cell-matrix adhesions - Converting tension into chemical signals. *Exp Cell Res,* 343**,** 35-41.

HYTÖNEN, V. P. & WEHRLE-HALLER, B. 2014. Protein conformation as a regulator of cell-matrix adhesion. *Phys Chem Chem Phys,* 16**,** 6342-57.

IZUMI, M., YAMADA, K. M. & HAYASHI, M. 1989. Vitronectin exists in two structurally and functionally distinct forms in human plasma. *Biochim Biophys Acta,* 990**,** 101-8.

JORGENSEN, W. L. & MADURA, J. D. 1983. Quantum and statistical mechanical studies of liquids. 25. Solvation and conformation of methanol in water. *Journal of the American Chemical Society,* 105**,** 1407-1413.

KANDOW, C. E., GEORGES, P. C., JANMEY, P. A. & BENINGO, K. A. 2007. Polyacrylamide hydrogels for cell mechanics: steps toward optimization and alternative uses. *Methods Cell Biol,* 83**,** 29-46.

KUO, J. C., HAN, X., HSIAO, C. T., YATES, J. R., 3RD & WATERMAN, C. M. 2011. Analysis of the myosin-II-responsive focal adhesion proteome reveals a role for beta-Pix in negative regulation of focal adhesion maturation. *Nat Cell Biol,* 13**,** 383-93.

LANGHE, R. P., GUDZENKO, T., BACHMANN, M., BECKER, S. F., GONNERMANN, C., WINTER, C., ABBRUZZESE, G., ALFANDARI, D., KRATZER, M. C., FRANZ, C. M. & KASHEF, J. 2016. Cadherin-11 localizes to focal adhesions and promotes cell-substrate adhesion. *Nat Commun,* 7**,** 10909.

LEHNERT, D., WEHRLE-HALLER, B., DAVID, C., WEILAND, U., BALLESTREM, C., IMHOF, B. A. & BASTMEYER, M. 2004. Cell behaviour on micropatterned substrata: limits of extracellular matrix geometry for spreading and adhesion. *J Cell Sci,* 117**,** 41-52.

LI, J., SU, Y., XIA, W., QIN, Y., HUMPHRIES, M. J., VESTWEBER, D., CABANAS, C., LU, C. & SPRINGER, T. A. 2017. Conformational equilibria and intrinsic affinities define integrin activation. *Embo j,* 36**,** 629-645.

LI, R., LUO, M., REN, M., CHEN, N., XIA, J., DENG, X., ZENG, M., YAN, K., LUO, T. & WU, J. 2014. Vitronectin regulation of vascular endothelial growth factor-mediated angiogenesis. *J Vasc Res,* 51**,** 110-7.

LUO, B. H., SPRINGER, T. A. & TAKAGI, J. 2003. Stabilizing the open conformation of the integrin headpiece with a glycan wedge increases affinity for ligand. *Proc Natl Acad Sci U S A,* 100**,** 2403-8.

MIERKE, C. T., KOLLMANNSBERGER, P., ZITTERBART, D. P., DIEZ, G., KOCH, T. M., MARG, S., ZIEGLER, W. H., GOLDMANN, W. H. & FABRY, B. 2010. Vinculin facilitates cell invasion into three-dimensional collagen matrices. *J Biol Chem,* 285**,** 13121-30.

NORDENFELT, P., ELLIOTT, H. L. & SPRINGER, T. A. 2016. Coordinated integrin activation by actin-dependent force during T-cell migration. *Nature Communications,* 7.

ORLANDO, R. A. & CHERESH, D. A. 1991. Arginine-glycine-aspartic acid binding leading to molecular stabilization between integrin alpha v beta 3 and its ligand. *J Biol Chem,* 266**,** 19543-50.

PANKOV, R. & YAMADA, K. M. 2002. Fibronectin at a glance. *J Cell Sci,* 115**,** 3861-3.

PINON, P., PÄRSSINEN, J., VAZQUEZ, P., BACHMANN, M., RAHIKAINEN, R., JACQUIER, M. C., AZIZI, L., MÄÄTTÄ, J. A., BASTMEYER, M., HYTÖNEN, V. P. & WEHRLE-HALLER, B. 2014. Talin-bound NPLY motif recruits integrin-signaling adapters to regulate cell spreading and mechanosensing. *J Cell Biol,* 205**,** 265-81.

PLOTNIKOV, S. V., PASAPERA, A. M., SABASS, B. & WATERMAN, C. M. 2012. Force fluctuations within focal adhesions mediate ECM-rigidity sensing to guide directed cell migration. *Cell,* 151**,** 1513-27.

PLOTNIKOV, S. V., SABASS, B., SCHWARZ, U. S. & WATERMAN, C. M. 2014. High-resolution traction force microscopy. *Methods Cell Biol,* 123**,** 367-94.

PREISSNER, K. T. & REUNING, U. 2011. Vitronectin in vascular context: facets of a multitalented matricellular protein. *Semin Thromb Hemost,* 37**,** 408-24.

PUKLIN-FAUCHER, E., GAO, M., SCHULTEN, K. & VOGEL, V. 2006. How the headpiece hinge angle is opened: New insights into the dynamics of integrin activation. *J Cell Biol,* 175**,** 349-60.

PYTELA, R., PIERSCHBACHER, M. D. & RUOSLAHTI, E. 1985. A 125/115-kDa cell surface receptor specific for vitronectin interacts with the arginine-glycine-aspartic acid adhesion sequence derived from fibronectin. *Proc Natl Acad Sci U S A,* 82**,** 5766-70.

RAHIKAINEN, R., VON ESSEN, M., SCHAEFER, M., QI, L., AZIZI, L., KELLY, C., IHALAINEN, T. O., WEHRLE-HALLER, B., BASTMEYER, M., HUANG, C. & HYTONEN, V. P. 2017. Mechanical stability of talin rod controls cell migration and substrate sensing. *Sci Rep,* 7**,** 3571.

ROCA-CUSACHS, P., GAUTHIER, N. C., DEL RIO, A. & SHEETZ, M. P. 2009. Clustering of alpha(5)beta(1) integrins determines adhesion strength whereas alpha(v)beta(3) and talin enable mechanotransduction. *Proc Natl Acad Sci U S A,* 106**,** 16245-50.

ROSSIER, O., OCTEAU, V., SIBARITA, J. B., LEDUC, C., TESSIER, B., NAIR, D., GATTERDAM, V., DESTAING, O., ALBIGÈS-RIZO, C., TAMPÉ, R., COGNET, L., CHOQUET, D., LOUNIS, B. & GIANNONE, G. 2012. Integrins β1 and β3 exhibit distinct dynamic nanoscale organizations inside focal adhesions. *Nat Cell Biol,* 14**,** 1057-67.

SALTEL, F., MORTIER, E., HYTÖNEN, V. P., JACQUIER, M. C., ZIMMERMANN, P., VOGEL, V., LIU, W. & WEHRLE-HALLER, B. 2009. New PI(4,5)P2- and membrane proximal integrin-binding motifs in the talin head control beta3-integrin clustering. *J Cell Biol,* 187**,** 715-31.

SCHILLER, H. B., FRIEDEL, C. C., BOULEGUE, C. & FÄSSLER, R. 2011. Quantitative proteomics of the integrin adhesome show a myosin II-dependent recruitment of LIM domain proteins. *EMBO Rep,* 12**,** 259-66.

SCHILLER, H. B., HERMANN, M. R., POLLEUX, J., VIGNAUD, T., ZANIVAN, S., FRIEDEL, C. C., SUN, Z., RADUCANU, A., GOTTSCHALK, K. E., THÉRY, M., MANN, M. & FÄSSLER, R. 2013. β1- and αv-class integrins cooperate to regulate myosin II during rigidity sensing of fibronectin-based microenvironments. *Nat Cell Biol,* 15**,** 625-36.

SCHINDELIN, J., RUEDEN, C. T., HINER, M. C. & ELICEIRI, K. W. 2015. The ImageJ ecosystem: An open platform for biomedical image analysis. *Mol Reprod Dev,* 82**,** 518-29.

SCHWARZ, U. S. 2017. Mechanobiology by the numbers: a close relationship between biology and physics. *Nat Rev Mol Cell Biol,* 18**,** 711-712.

SHIKATA, Y., RIOS, A., KAWKITINARONG, K., DEPAOLA, N., GARCIA, J. G. & BIRUKOV, K. G. 2005. Differential effects of shear stress and cyclic stretch on focal adhesion remodeling, site-specific FAK phosphorylation, and small GTPases in human lung endothelial cells. *Exp Cell Res,* 304**,** 40-9.

SOLDI, R., MITOLA, S., STRASLY, M., DEFILIPPI, P., TARONE, G. & BUSSOLINO, F. 1999. Role of alphavbeta3 integrin in the activation of vascular endothelial growth factor receptor-2. *EMBO J,* 18**,** 882-92.

STRICKER, J., ARATYN-SCHAUS, Y., OAKES, P. W. & GARDEL, M. L. 2011. Spatiotemporal constraints on the force-dependent growth of focal adhesions. *Biophys J,* 100**,** 2883-93.

SU, Y., XIA, W., LI, J., WALZ, T., HUMPHRIES, M. J., VESTWEBER, D., CABANAS, C., LU, C. & SPRINGER, T. A. 2016. Relating conformation to function in integrin alpha5beta1. *Proc Natl Acad Sci U S A,* 113**,** E3872-81.

THIEVESSEN, I., THOMPSON, P. M., BERLEMONT, S., PLEVOCK, K. M., PLOTNIKOV, S. V., ZEMLJIC-HARPF, A., ROSS, R. S., DAVIDSON, M. W., DANUSER, G., CAMPBELL, S. L. & WATERMAN, C. M. 2013. Vinculin-actin interaction couples actin retrograde flow to focal adhesions, but is dispensable for focal adhesion growth. *J Cell Biol,* 202**,** 163-77.

VAN DER SPOEL, D., LINDAHL, E., HESS, B., GROENHOF, G., MARK, A. E. & BERENDSEN, H. J. 2005. GROMACS: fast, flexible, and free. *J Comput Chem,* 26**,** 1701-18.

WENNERBERG, K., LOHIKANGAS, L., GULLBERG, D., PFAFF, M., JOHANSSON, S. & FASSLER, R. 1996. Beta 1 integrin-dependent and -independent polymerization of fibronectin. *J Cell Biol,* 132**,** 227-38.

WEST, X. Z., MELLER, N., MALININ, N. L., DESHMUKH, L., MELLER, J., MAHABELESHWAR, G. H., WEBER, M. E., KERR, B. A., VINOGRADOVA, O. & BYZOVA, T. V. 2012. Integrin beta3 crosstalk with VEGFR accommodating tyrosine phosphorylation as a regulatory switch. *PLoS One,* 7**,** e31071.

YANG, J. T., BADER, B. L., KREIDBERG, J. A., ULLMAN-CULLERÉ, M., TREVITHICK, J. E. & HYNES, R. O. 1999. Overlapping and independent functions of fibronectin receptor integrins in early mesodermal development. *Dev Biol,* 215**,** 264-77.

YEUNG, T., GEORGES, P. C., FLANAGAN, L. A., MARG, B., ORTIZ, M., FUNAKI, M., ZAHIR, N., MING, W., WEAVER, V. & JANMEY, P. A. 2005. Effects of substrate stiffness on cell morphology, cytoskeletal structure, and adhesion. *Cell Motil Cytoskeleton,* 60**,** 24-34.

ZAIDEL-BAR, R., ITZKOVITZ, S., MA'AYAN, A., IYENGAR, R. & GEIGER, B. 2007a. Functional atlas of the integrin adhesome. *Nat Cell Biol,* 9**,** 858-67.

ZAIDEL-BAR, R., MILO, R., KAM, Z. & GEIGER, B. 2007b. A paxillin tyrosine phosphorylation switch regulates the assembly and form of cell-matrix adhesions. *J Cell Sci,* 120**,** 137-48.

ZAMIR, E., KATZ, M., POSEN, Y., EREZ, N., YAMADA, K. M., KATZ, B. Z., LIN, S., LIN, D. C., BERSHADSKY, A., KAM, Z. & GEIGER, B. 2000. Dynamics and segregation of cell-matrix adhesions in cultured fibroblasts. *Nat Cell Biol,* 2**,** 191-6.

ZHANG, C., LIU, J., JIANG, X., HAYDAR, N., SHAN, H. & ZHU, J. 2013. Modulation of integrin activation and signaling by alpha1/alpha1'-helix unbending at the junction. *J Cell Sci,* 126**,** 5735-47.

ZHU, J., LUO, B. H., XIAO, T., ZHANG, C., NISHIDA, N. & SPRINGER, T. A. 2008. Structure of a complete integrin ectodomain in a physiologic resting state and activation and deactivation by applied forces. *Mol Cell,* 32**,** 849-61.

ZHU, J. & SPRINGER, T. A. 2013. Complete integrin headpiece opening in eight steps. *J Cell Biol,* 201**,** 1053-68.